Genomically Complex Human Angiosarcoma and Canine Hemangiosarcoma Establish Convergent Angiogenic Transcriptional Programs Driven by Novel Gene Fusions

Jong Hyuk Kim[1,2,3,4*], Kate Megquier[5], Rachael Thomas[6], Aaron L. Sarver[1,3,7], Jung Min Song[3], Yoon Tae Kim[8], Nuojin Cheng[9,a], Ashley J. Schulte[1,2,3], Michael A. Linden[1,3,10], Paari Murugan[1,3,10], LeAnn Oseth[3], Colleen L. Forster[11], Ingegerd Elvers[5,12], Ross Swofford[5], Jason Turner-Maier[5], Elinor K. Karlsson[5,13], Matthew Breen[6,14], Kerstin Lindblad-Toh[5,12], Jaime F. Modiano[1,2,3,4,10,15,16]

[1]Animal Cancer Care and Research Program, University of Minnesota, St Paul, MN, USA

[2]Department of Veterinary Clinical Sciences, College of Veterinary Medicine, University of Minnesota, St Paul, MN, USA

[3]Masonic Cancer Center, University of Minnesota, Minneapolis, MN, USA

[4]Institute for Engineering in Medicine, University of Minnesota, Minneapolis, MN, USA

[5]Broad Institute of Harvard and MIT, Cambridge, MA, USA

[6]Department of Molecular Biomedical Sciences, College of Veterinary Medicine & Comparative Medicine Institute, North Carolina State University, Raleigh, NC, USA

[7]Institute for Health Informatics, University of Minnesota, Minneapolis, MN, USA

[8]Department of Electrical Engineering and Computer Science, York University, Toronto, Ontario, Canada

[9]School of Mathematics, College of Science and Engineering, University of Minnesota, Minneapolis, MN, USA

[10]Department of Laboratory Medicine and Pathology, School of Medicine, University of Minnesota, Minneapolis, MN, USA

24 [11]The University of Minnesota Biological Materials Procurement Network (BioNet), University
25 of Minnesota, Minneapolis, MN, USA
26 [12]Science for Life Laboratory, Department of Medical Biochemistry and Microbiology, Uppsala
27 University, Uppsala, Sweden
28 [13]University of Massachusetts Medical School, Worcester, MA, USA
29 [14]Cancer Genetics Program, University of North Carolina Lineberger Comprehensive Cancer
30 Center, Raleigh, NC, USA
31 [15]Center for Immunology, University of Minnesota, Minneapolis, MN, USA
32 [16]Stem Cell Institute, University of Minnesota, Minneapolis, MN, USA
33 [a]Current address: Applied Mathematics, University of Colorado Boulder, Boulder, CO, USA
34
35 **Running Title**: Angiogenic transcription programs in angiosarcoma
36
37 **Keywords**: Angiosarcoma, chromosome translocation, fusion gene, hemangiosarcoma, *TP53*
38
39 **Corresponding Author**: Jong Hyuk Kim (jhkim@umn.edu), MCRB560A, Masonic Cancer
40 Center, 420 Delaware St. SE, Minneapolis, MN 55455. Phone: 612-624-3612, Email:
41 jhkim@umn.edu
42
43
44
45
46

Abstract

Sporadic angiosarcomas (ASs) are aggressive vascular sarcomas whose rarity and genomic complexity present significant obstacles in deciphering the pathogenic significance of individual genetic alterations. Numerous fusion genes have been identified across multiple types of cancers, but their existence and significance remain unclear in sporadic ASs. In this study, we leveraged RNA sequencing data from thirteen human ASs and 76 spontaneous canine hemangiosarcomas (HSAs) to identify fusion genes associated with spontaneous vascular malignancies. Ten novel protein-coding fusion genes, including *TEX2-PECAM1* and *ATP8A2-FLT1*, were identified in seven of the thirteen human tumors, with two tumors showing mutations of *TP53*. *HRAS* and *NRAS* mutations were found in ASs without fusions or *TP53* mutations. We found fifteen novel protein-coding fusion genes including *MYO16-PTK2*, *GABRA3-FLT1*, and *AKT3-XPNPEP1* in eleven of the 76 canine HSAs; these fusion genes were seen exclusively in tumors of the angiogenic molecular subtype that contained recurrent mutations in *TP53*, *PIK3CA*, *PIK3R1*, and *NRAS*. In particular, fusion genes and mutations of *TP53* co-occurred in tumors with higher frequency than expected by random chance, and they enriched gene signatures predicting activation of angiogenic pathways. Comparative transcriptomic analysis of human ASs and canine HSAs identified shared molecular signatures associated with activation of PI3K/AKT/mTOR pathways. Our data show that, while driver events of malignant vasoformative tumors of humans and dogs include diverse mutations and stochastic rearrangements that create novel fusion genes, convergent transcriptional programs govern the highly conserved morphological organization and biological behavior of these tumors in both species.

70 **Introduction**

71 Sarcomas are diverse tumors that arise from cells of mesenchymal origin in soft tissues
72 such as blood and lymphatic vessels, fat, bone, cartilage, muscle, and connective tissues. The
73 heterogeneity of sarcomas has provided an impetus for developing molecular approaches to
74 classify these tumors (1,2), leading to their categorization into genomically simple and
75 genomically complex sarcomas (1,3). Angiosarcomas (ASs) are rare, highly aggressive,
76 genomically complex sarcomas of blood vessel-forming cells (3,4). The five-year survival rate of
77 AS is approximately 40% (5-7), but half of patients have metastatic or unresectable disease with
78 a median overall survival of less than 6 months (8). The events that drive progression are
79 incompletely understood; previous studies have identified recurrent mutations of *RAS*, *PTPRB*,
80 *PLCG1*, *KDR* (kinase insert domain receptor, also known as *VEGFR2*), *TP53*, *PIK3CA*, and
81 *FLT4* (*VEGFR3*) in human ASs (9-12). *MYC* gene amplification and alterations in the TP53,
82 CDKN2, NF-κB/IL-6, PIK3CA/AKT/mTOR pathways have also been reported (13); however,
83 these studies represent a small case series, precluding definitive conclusions regarding
84 pathogenic mechanisms that contribute to the genetic cause and to the progression of the disease.

85 Hemangiosarcoma (HSA) is a malignant vascular tumor that is common in dogs with an
86 estimated tens of thousands of cases diagnosed each year (14-16). Canine HSA shares clinical
87 and morphological features with human AS, as well as aspects of its mutational landscape (17-
88 20). We previously documented three molecular subtypes of HSA, characterized by angiogenic,
89 inflammatory, and adipogenic transcriptomic signatures (21). These gene expression signatures
90 are conserved in HSA progenitor cells that show multipotency and self-renewal (21).
91 Nevertheless, the transcriptional state of these HSA progenitor cells seems to be somewhat
92 malleable, regulated by immune and metabolic reprogramming (22). Mutations in genes that

93 regulate genomic integrity, such as *TP53,* can alter the intrinsic transcriptional program of tumor
94 cells; however, genomic instability in the tumor can create even more dramatic changes by
95 modulating transcriptional programs of heterotypic stromal cells in the tumor tissue, as well as in
96 the composition of the niche (23,24).

97 Chromosome translocations and the resulting fusion genes are important contributors to
98 the pathogenesis of cancer, particularly in sarcomas and hematopoietic malignancies (25).
99 However, the nature and frequency of these events in canine HSA and human AS remains
100 unclear. Here, we used next generation RNA sequencing (RNA-Seq) data to identify fusion
101 genes in thirteen human ASs and 76 visceral HSAs originating from 74 dogs, and we
102 investigated the relationship of these fusions to the mutational landscape of the tumor. We
103 identified ten novel protein-coding fusion genes including *TEX2-PECAM1* and *ATP8A2-FLT1* in
104 seven of thirteen human ASs, and two of the fusion-detected tumors showed mutations of *TP53*
105 (R248Q and P250L). In canine HSAs, we found novel protein-coding fusion genes in a subset of
106 the tumors of the angiogenic subtype. These fusion genes co-occurred with *TP53* mutations and
107 were associated with gene enrichment for activated angiogenic pathways in the tumors. Our data
108 suggest that genomic instability induced by mutations of *TP53* creates a permissive environment
109 for fusion genes, with selection for angiogenic molecular programs in malignant vasoformative
110 tumors. Our data also demonstrate that human AS and canine HSA maintain molecular programs
111 that activate convergent signaling pathways to establish angiogenic phenotypes despite their
112 genomic complexity.
113

114 **Materials and Methods**

115 **Human tissue samples**

116 Snap frozen and formalin fixed paraffin embedded (FFPE) tissues for human biospecimens were
117 obtained from the University of Minnesota Biological Materials Procurement Network (UMN
118 BioNet) and from the Cooperative Human Tissue Network (CHTN) under their standardized
119 patient consent protocols. The demographic characteristics of human patients from whom we
120 obtained ASs (*n* = 13) and normal tissue samples (*n* = 6) are summarized in **Supplementary**
121 **Table S1**.
122
123 **Dog tissue samples**
124 Seventy-six snap frozen and FFPE tissue samples were obtained from 74 dogs with HSAs.
125 Frozen and FFPE tissues samples from 10 dogs with splenic hematomas, which are benign
126 lesions with enlarged vascular spaces lined by endothelial cells, were used as controls. Samples
127 were obtained as part of medically necessary diagnostic procedures and were used for research
128 with owner consent. The origin of these samples was reported previously (14,21,26-28), or they
129 were collected from dogs with HSA or with splenic hematomas at the Veterinary Medical
130 Center, University of Minnesota. Procedures involving animal use were done with approval and
131 under the supervision of the University of Minnesota Animal Care and Use Committee
132 (protocols 1110A06186, 1507-32804A, 0802A27363, 1101A94713, 1312-31131A, and 1702-
133 34548A). The demographic characteristics of dogs (*n* = 74) from whom we acquired HSA and
134 non-malignant splenic hematomas (*n* = 10) are summarized in **Supplementary Table S2**.
135
136 **Histological assessment**
137 FFPE sections (4 µm) were stained with hematoxylin and eosin (H&E) and examined by
138 veterinary pathologists to assign a histological diagnosis of canine HSA. Solid, capillary,

139 cavernous, or mixed histological subtypes were assigned using accepted criteria (29); mitotic
140 index (MI) was calculated per 1,000 cells in 5-10 random fields under 400X magnification (30).
141 H&E slides were further reviewed for tumor content by two board-certified medical pathologists
142 (ML and PM) (31), with the percent of sample containing viable nucleated cells corresponding to
143 tumor recorded in a range of 0 to > 90% based on the planar surface of the sections. Diagnostic
144 and histopathology reports of human tissues were provided by the specimen providers, the UMN
145 BioNet and the CHTN.
146
147 **RNA isolation and generation of RNA-Seq libraries**
148 Total RNA was isolated from tissue samples using the TriPure Isolation Reagent (Roche Applied
149 Science, Indianapolis, IN, USA). The RNeasy Mini Kit (Qiagen, Valencia, CA, USA) was used
150 for clean-up according to the manufacturer's instructions. RNA-Seq from 74 canine HSA tissues
151 is published (17,21,32,33) and an additional data set was generated from two canine HSA tissues
152 and from 10 non-malignant splenic hematoma tissues. Total RNA was also extracted from 13
153 human AS tissues and from six normal tissues. Two µg of total RNA from each sample were
154 quantified and assessed for quality; RNA-Seq libraries were generated as described (21) using
155 the TruSeq RNA sample preparation kit (Illumina Inc., San Diego, CA). Sequencing was
156 performed using HiSeq 2000 or 2500 systems (Illumina Inc.). Each sample was sequenced to a
157 targeted depth of 20 – 80 million paired-end reads with mate-pair distance of 50 bp. Primary
158 analysis and demultiplexing were performed using CASAVA software version 1.8.2 (Illumina
159 Inc.) to verify the quality of the sequence data. The end result of the CASAVA workflow was
160 demultiplexed into FASTQ files for analysis. Bioanalyzer quality control and RNA-Seq were
161 performed at the University of Minnesota Genomics Center (UMGC) or at the Broad Institute.

162

163 **Bioinformatics analysis**

164 The original FASTQ files prepared from thirteen human ASs and six non-malignant tissues were
165 mapped to the human reference genome (GRCh38). The FASTQ files generated from 76 canine
166 HSAs and ten non-malignant splenic hematomas were mapped to the dog reference genome
167 (Canfam3.1). Sequencing quality was assessed by FastQC. The deFuse algorithm (34) was used
168 to identify putative fusion events. To discriminate true fusion candidates from artifacts, we
169 included fusion events with exon boundaries in both fusion partners and excluded events created
170 from adjacent genes that showed breakpoint homology (>1). We also filtered highly recurrent
171 fusion events that were found at implausible frequencies across tumor and non-malignant tissue
172 samples (35) and transcription-induced chimeras. The split sequences of the fusion genes were
173 validated by *de novo* assembly using Trinity (36). TranscriptsToOrfs and deFuse-Trinity tools
174 verified the deFuse fusion predictions with Trinity-assembled transcripts and open reading
175 frames. TopHat2 was used to generate BAM files, and the Integrative Genomics Viewer (IGV
176 2.3; Broad Institute, Cambridge, MA) was used to visualize the mate pair sequences of fusion
177 genes. A protein translation tool in Expert Protein Analysis System (ExPASy; SIB Swiss
178 Institute of Bioinformatics, Lausanne, Switzerland) was used to determine in-frame fusion
179 proteins. Tumor purity and microenvironment scores were assessed using the bioinformatics
180 tools ESTIMATE (37) and *xCell* (38).

181

182 **Reverse transcription polymerase chain reaction (RT-PCR) and Sanger sequencing**

183 RT-PCR was performed to validate fusion transcripts identified by deFuse (39). Briefly, cDNA
184 was synthesized using SuperScript® VILO cDNA Synthesis Kit and Master Mix (Invitrogen).

185 PCR amplification was performed using a conventional thermocycler with HotStarTaq DNA
186 polymerase (Qiagen) or using a LightCycler® 96 (Roche Applied Science, Indianapolis, IN,
187 USA) with FastStart SYBR Green Master Mix (Roche Applied Science) for quantitative real-
188 time RT-PCR (40). PCR primer pairs used for fusion gene amplification are presented in the
189 Results section. *GAPDH* was used as a control for RNA integrity and for the RT-PCR reactions.
190 The forward and reverse primer sequences for *GAPDH* were 5'-GGA GTC CAC TGG CGT
191 CTT CAC-3' and 5'-GAG GCA TTG CTG ATG ATC TTG AGG-3', respectively. Relative
192 mRNA values were expressed as delta-Ct values normalized to *GAPDH*. Sanger sequencing was
193 performed at the UMGC.
194
195 **Fluorescence *in situ* hybridization (FISH)**
196 FISH was performed to detect *MYO16-PTK2* and *GABRA3-FLT1* fusion genes by designing
197 FISH probes derived from the genome-anchored canine CHORI-82 bacterial artificial
198 chromosome (BAC) library (41). Single locus probes were used for proximal *MYO16* at dog
199 chromosome (CFA) 22:57,565,917-57,750,789 (clone 183H20), distal *MYO16* at CFA
200 22:57,750,801-57,967,880 (clone 385H13), and *PTK2* at CFA 13:35,302,679-35,483,060 (clone
201 451H13) with distinct fluorescent tags. For *GABRA3-FLT1* fusion, break-apart FISH probes
202 were used for proximal *FLT1* at CFA 25:11,057,892-11,263,935 (clone 363B20) and distal *FLT1*
203 at CFA 25:11,274,078-11,471,538 (clone 235H9). The PureLink® HiPure Plasmid Maxiprep Kit
204 (Invitrogen) was used for BAC DNA extraction. For preparation and hybridization of FISH
205 probes, BAC DNA probes were labeled by Nick Translation Kit (Abbott Molecular) using
206 Green-500 dUTP, Orange-552 dUTP and Aqua-431 dUTP (Enzo Life Science). Labeled DNA
207 was precipitated in COT-1 DNA, salmon sperm DNA, sodium acetate and 95% ethanol, then

208 dried and resuspended in 50% formamide hybridization buffer. The Red-proximal *MYO16*,
209 Green-distal *MYO16* and Aqua-*PTK2* probes were combined into one 3-color FISH probe for
210 *MYO16-PTK2* fusion. The Red-proximal *FLT1* and Green-distal *FLT1* break-apart probes were
211 applied for the split *FLT1* gene.

212 FFPE sections (4 µm) were processed according to the Dako IQFISH protocol; probes
213 were applied to the slide and hybridized for 24 hours at 37°C in a humidified chamber. After
214 hybridization, slides were washed and counterstained with DAPI. Fluorescent signals were
215 visualized on an Olympus BX61 microscope workstation (Applied Spectral Imaging, Vista, CA)
216 with DAPI, FITC, Texas Red and Aqua filter sets. FISH images were captured using an
217 interferometer-based CCD cooled camera (ASI) and FISHView ASI software. A total of 200
218 interphase cells were examined for each sample. Non-malignant canine spleen tissues were used
219 as controls for the FISH experiment.

220

221 **Validation of somatic mutations using RNA-Seq data**

222 A pipeline was developed to identify the bases present at locations defined as somatic mutations
223 in the Tumor-Normal exome calls (17). Briefly, RNA-Seq data were mapped using the STAR-
224 Mapper (42) with STAR-FUSION mapping settings (43) to the Canfam3.1 or GRCh38 genome.
225 BAM files generated by STAR were sorted and indexed using Samtools (44). Starting from a file
226 containing somatic mutation locations and a file containing a list of BAM file locations, the
227 pipeline uses Samtools (44) functions to identify the bases present at each location at each file
228 and then reports whether a variant is found at that location. For inclusion within the variant file,
229 at least one sample must have at least 3 reads that support the variant and that represent greater
230 than 10% of all reads at that location.

231

232 **Gene expression profiling**

233 CLC Bio Genomics Workbench 10 (CLC Bio, Aarhus, Denmark) and DESeq2 R packages were
234 used to quantify gene expression and differential gene expression analysis as described (45).
235 Briefly, paired-end RNA-Seq data with mate-pair distance of 50 bp in FASTQ format were
236 imported, and sequencing quality was determined. Transcriptomics analysis was then performed
237 to generate the expression level of each gene presented as total reads by mapping the sequencing
238 reads to Canfam3.1 or GRCh38. Heatmaps and hierarchical clustering based on average linkage
239 were visualized using Cluster 3.0, Morpheus (https://clue.io/morpheus), or R packages. GO
240 Enrichment Analysis (46-48) or Ingenuity® Pathway Analysis software version 8.6 (Qiagen,
241 Redwood City, CA) were used to define biological functions, canonical pathways, and upstream
242 regulators associated with differently expressed genes (DEGs) between groups using Benjamini-
243 Hochberg multiple testing corrections to evaluate significance. For gene expression profiling,
244 unsupervised PCA and hierarchical clustering were performed to define subtypes of canine
245 HSAs as described previously (21). Gene expression data of human sarcomas in The Cancer
246 Genome Atlas (TCGA) database were also compared with our data sets.

247

248 **TMA generation and immunohistochemistry (IHC)**

249 Canine TMA blocks were generated from 45 HSA tissues, including 32 tumors used for RNA-
250 Seq and eight non-tumor tissues (six splenic hematomas and two non-malignant liver samples).
251 Tissue cores of 1-mm diameter in quadruplicate from each sample were assembled in random
252 order in four TMA blocks. One TMA block with mouse tissues was generated for staining
253 controls. Immunostaining with CD31, Vimentin and Pan-Cytokeratin antibodies was evaluated to

254 support tumor content estimates. A human TMA block was generated from ten AS tissues and
255 six non-malignant tissues (submandibular gland, skin, breast adipose tissue, thigh skeletal
256 muscle, spleen, and lung).

257 Unstained TMA sections (4 µm) were de-paraffinized and rehydrated using standard
258 methods for IHC. All of the immunohistochemical assays, including validation for antibodies,
259 were performed and optimized at the UMN BioNet Histology Laboratory or the Veterinary
260 Diagnostic Laboratory at the University of Minnesota. Antibodies used for IHC are summarized
261 in **Supplementary Table S3**. The immunostaining score assigned to each case was a
262 semiquantitative assessment derived from the product of two integers, ranging from 0 to 3 and
263 from 1 to 3, that respectively reflect the percentage of positive cells in a sample and the intensity
264 of staining at high power magnification (400X) as described previously with some modifications
265 (49). The percentage of positive cells was scored from 0 to 3+, where 0 reflected specific
266 staining in <1% of the cells, 1+ reflected specific staining in >1% and <25% of the cells, 2+
267 reflected specific staining in 25–75% of the cells, and 3+ reflected specific staining in >75% of
268 the cells. The intensity was assessed as weak (intensity score 1), moderate (intensity score 2), or
269 strong (intensity score 3). Immunostaining results were scored (ranging from 0 to 9) by
270 multiplying the percentage of positive cells (score 0-3) by the intensity (score 1-3).
271

272 **Statistical analysis**

273 Chi-square or Fisher's exact test, was performed for contingency tables analysis. Continuous
274 values were analyzed by Welch's (Heteroscedastic) T-test or Mann-Whitney U test. The
275 statistical tests were two-tailed. Statistical analysis was performed using GraphPad Prism 6
276 (GraphPad Software, Inc., San Diego, CA). *P*-values are reported without inference of

277 significance, consistent with the American Statistical Association's Statement on Statistical
278 Significance and P-Values (50).
279
280 **Results**
281
282 **Novel protein-coding fusion genes are identified in human ASs and canine HSAs**
283 Putative fusion gene events were identified from RNA-Seq data as paired-end sequence reads
284 that mapped connecting two distant genes (**Supplementary Fig. S1A**). We identified novel in-
285 frame protein-coding fusion transcripts for ten fusion events in 7 of 13 (53.8%) human ASs **(Fig.**
286 **1A**; **Table 1)**. Two of the fusions were inter-chromosomal events and eight were intra-
287 chromosomal events. The fusions included *TEX2-PECAM1*, which contained the gene that
288 encodes CD31, and *ATP8A2-FLT1*, a kinase fusion gene that encodes the vascular endothelial
289 growth factor receptor 1 (VEGFR1). None of the ten fusion events was seen in more than one
290 tumor, and three of the seven fusion-positive tumors contained two distinct fusion events each.
291 In canine HSA, we found fifteen novel protein-coding fusion genes in eleven of 76
292 tumors (14.5%) (**Fig. 1B**; **Table 2**). Ten of the fusions were inter-chromosomal events and five
293 were intra-chromosomal events. None of the fifteen fusion events was seen in more than one
294 tumor, and four of the eleven fusion-positive tumors involved two distinct fusion genes each.
295 One fusion partner in four of the translocations encoded either a protein kinase or a protein
296 phosphatase associated with angiogenic signaling (*MYO16-PTK2, GABRA3-FLT1*, *AKT3-*
297 *XPNPEP1,* and *PTPRB-NOL10*). Eight of the fusion genes were associated with kinase signaling
298 or kinase binding activity, such as PI3 kinase signaling, a MAP kinase, a receptor tyrosine
299 kinase, a protein serine/threonine kinase, and an NAD+ kinase. Gene ontology annotations of the

300 fusion partners for every translocation are described in **Supplementary Table S4** for human AS
301 and **Supplementary Table S5** for canine HSA. Fusion genes were not present in any of the
302 human non-malignant tissues (n = 6) or canine hematomas (n = 10) examined. Conserved driver
303 translocations such as *BCR-ABL* and *MYC-IGH* that are present in both human and canine
304 chronic myelogenous leukemia and Burkitt lymphoma, respectively (51), were not identified in
305 human AS and canine HSA. All the fusion events identified in the seven human ASs and eleven
306 canine HSAs involved different gene pairs, with the exception of the *FLT1* gene, which created
307 fusions with a different partner gene in one case from each species.

308 To determine whether the non-tumor components in the tumor tissue affected the
309 detection of fusion genes, we quantified tumor content histologically and bioinformatically in
310 canine HSAs **(Supplementary Fig. S2A - E**). Seventy of the 76 HSA samples were
311 histologically evaluated, and the tumor content was not different between HSA samples with
312 fusion events (n = 11) and those without fusion events (n = 59). We used two independent
313 bioinformatic tools, *xCell* and ESTIMATE, to predict stromal and immune cell components, and
314 these algorithms generated consistent output scores (Pearson's $R = 0.84$; $R^2 = 0.71$; $P < 0.00001$)
315 that showed the presence of fusion genes was not associated with tumor purity. The detection of
316 fusion genes was also independent of sequencing depth (**Supplementary Fig. S2F**). To rule out
317 artifacts from the computational process, we validated the presence of the inter-chromosomal
318 fusion gene, *SCLT1-NIPBL,* in the original human AS sample where it was identified, in two
319 additional samples where it was undetectable based on sequencing data, and in a non-malignant
320 tissue sample. The fusion transcript was detectable by quantitative real time RT-PCR
321 amplification; PCR primer pairs were designed to amplify putative split sequences (up to 200
322 base pairs) involving the breakpoints identified by deFuse (**Supplementary Fig. S3A**). We

323 confirmed that the junction sequences between the two genes producing the new fusion event
324 were amplified by PCR (**Supplementary Fig. S3B**). Four representative fusion transcripts found
325 in canine HSAs (*MYO16-PTK2*; *AKT3-XPNPEP1*; *AP4E1-BAIAP2*; *NOL10-PTPRB*) were also
326 detected, but only in the respective cases where they were identified in the sequencing data
327 (**Supplementary Fig. S3C - E**). Each PCR amplification product was verified by Sanger
328 sequencing. We then used RT-PCR to evaluate RNA-Seq data from 63 canine tissue samples (53
329 HSAs and 10 hematomas) for the presence of these four fusion transcripts. The results were
330 consistent between RNA-Seq and PCR, as we found neither false-positive nor false-negative
331 events in the samples tested (**Supplementary Table S6**).
332
333 **Fusion genes are associated with DNA copy number variations**
334 We then determined if any of the fusion partner genes identified in our analysis were associated
335 with DNA copy number alterations. Publicly available whole Exome-sequencing data generated
336 from an independent data set of 36 human patients with ASs was used (12). Copy number
337 variations were found in twelve of the twenty (60%) fusion partner genes: nine genes were
338 amplified, and five genes were deleted (**Fig. 1C**; **Supplementary Fig. S4)**. *TEX2* (39%),
339 *STEAP1B* (25%) and *PECAM1* (25%) were the top three genes where copy number gains
340 occurred most frequently. For canine HSA, we used oligonucleotide array comparative genomic
341 hybridization (oaCGH) in a larger HSA dataset (n = 123) (19). Copy number gains were
342 observed in 29 of the 30 (96.7%) fusion partners, and copy number losses were observed in 27 of
343 the 30 (90.0%) fusion partners. Protein kinase-encoding genes, *PTK2*, *FLT1*, and *AKT*3 revealed
344 a higher frequency of copy number gain: 15.5% gain vs 0.8% loss for *PTK2*; 4.9% gain vs 0.8%
345 loss for *FLT1*; and 4.1% gain vs 0.8% loss for *AKT3*, suggesting that copy number alterations

346 leading to dysregulation of downstream kinase signaling contribute at least partly to the
347 angiogenic program in a subset of canine HSAs (**Fig. 1D**).
348
349 **Chromosomal translocations resulting in fusion genes are detectable in canine HSAs**
350 We performed FISH to confirm that fusion genes were generated by chromosome translocations.
351 We chose representative inter-chromosomal fusions, *MYO16-PTK2* and *GABRA3-FLT1* for
352 cytogenetic validation because PTK2 and VEGFR1 are key molecules that regulate pathogenic
353 signaling in vascular cancers, including canine HSA (52). **Fig. 2A** illustrates the predicted
354 structure of *MYO16-PTK2* inter-chromosomal fusion between CFA 22 and CFA 13, based on
355 deFuse and Sanger sequencing data (**Fig. 2B**). The predicted fusion gene comprises exons 1-32
356 of *MYO16* (CFA 22) and exons 12-31 of *PTK2* (CFA 13), with the putative junction joining
357 *MYO16* exon 32 and *PTK2* exon 12. Breakage occurs between exons 32 and 33 of *MYO16* at
358 CFA 22:57,750,807 bp, and between exons 11 and 12 of *PTK2* at CFA 13:35,397,284 bp.
359 Independent FISH probes identifying the association between proximal and distal *MYO16* and
360 the breakpoint of *PTK2* (**Fig. 2C**) confirmed the presence of the *MYO16-PTK2* fusion gene
361 between CFA 22 and 13 in archival FFPE samples from the same dog tumor. The *MYO16-PTK2*
362 fusion was identified by deFuse and RT-PCR (**Fig. 2D**). The t(CFA 13;CFA 22) translocation
363 was present in interphase nuclei of 16.8% of the tumor cells, with a smaller subpopulation
364 showing amplification of the fusion (**Fig. 2E**).
365 We used break-apart FISH to validate the presence of the *GABRA3-FLT1* fusion gene
366 (**Fig. 2F**). Split *FLT1* probes were found in 36.7% of tumor cells in archival FFPE samples from
367 the dog tumor in which the *GABRA3-FLT1* fusion was identified by deFuse and RT-PCR.
368 Interestingly, in this tumor the intact *FLT1* gene showed consistent amplification (up to four

369 copies), suggesting Flt-1 (also known as VEGFR1) activation in this tumor might have occurred
370 through multiple mechanisms (**Fig. 2G**). We next used FISH analysis to assess recurrence of the
371 *MYO16-PTK2* fusion in a tissue microarray (TMA) comprised of 45 visceral HSAs and eight
372 non-malignant tissues (six spleens; two livers). The *MYO16-PTK2* fusion was once again present
373 in the sample from the canine tumor in which it was discovered, but it was not seen in any other
374 sample on the TMA. We also performed FISH to detect the *ATP8A2-FLT1* fusion in human AS
375 using a break-apart *FLT1* probe, but the fusion was undetectable in our FFPE sample. This might
376 have been due to the small number of tumor cells that were likely to contain the fusion event in a
377 heterogeneous clonal population. Since none of the fusion transcripts identified in our cohorts of
378 human and canine tumors were recurrent, we sought to determine if the fusion events were
379 associated with other genetic and molecular programs.
380
381 **Fusion genes and somatic variants in human ASs enrich angiogenic gene signatures**
382 To examine genomic aberrations associated with the fusion genes, we determined somatic
383 variations and gene expression profiles using RNA-Seq data. In human ASs, *TP53* mutations
384 (R248Q and P250L) were observed in two of thirteen human ASs, which also had fusion genes
385 (*SMURF1-TMEM139* and *AGO2-TRAPPC9* in one tumor, *IRF9-THTPA* in the other tumor).
386 *NRAS* (Q61L; $n = 1$) or *HRAS* (Q61L; $n = 1$) mutations were also detected, and both were present
387 in tumors that did not have fusion genes or *TP53* mutations (**Fig. 3A**; **Table 1**). The RNA-Seq
388 data did not provide evidence of mutations in *PIK3CA, PTEN*, or *KRAS* in this group of thirteen
389 ASs.
390 We established transcriptomic profiles of human ASs to identify molecular traits that
391 regulate global gene expression. We identified 1,237 differentially expressed genes between ASs

392 (n = 13) and non-malignant controls (N = 6) (FDR P-value < 0.05): 490 genes were upregulated
393 and 747 genes were downregulated in ASs. Biological functions and pathway analysis revealed
394 that upregulated genes in ASs were associated with cancer, angiogenesis, vasculogenesis, and
395 development of vasculature (P < 0.00001) (**Supplementary Table S7**). Additionally, we
396 performed cell type enrichment analysis using the *xCell* tool (38) to predict relative populations
397 of cellular components that comprised the AS tissues (**Supplementary Fig. S5**). We compared
398 the cell type signature of AS with that of sarcomas (n = 263) from the TCGA database, which
399 did not include AS. The results showed that gene signatures associated with endothelial cells and
400 activated dendritic cells were highly enriched in ASs, while other sarcomas in the TCGA
401 revealed gene enrichment of smooth muscle cells. Gene expression profiles of non-malignant
402 samples indicated distinct tissue-specific patterns of submandibular gland, skin, breast adipose
403 tissue, thigh skeletal muscle, spleen, and lung. The ASs showed upregulation of key angiogenic
404 genes such as *PECAM1* (*CD31*), *FLT1* (*VEGFR1*), *KDR* (*VEGFR2)*, and *FLT4* (*VEGFR3)*
405 compared to non-malignant tissues (**Fig. 3B**). In addition, 6 of 20 (30.0%) fusion partners
406 (including *PECAM1*) showed a higher level of expression in the tumors compared to non-
407 malignant tissues (P < 0.05; fold change in a range from 1.9 to 35.0) (**Fig. 3C**). Collectively, our
408 data showed enriched angiogenic molecular programs were present in human ASs. Furthermore,
409 both tumors with *TP53* mutations also harbored fusion genes.
410

411 **Fusion genes that co-occur with mutations of *TP53* are present exclusively in angiogenic**
412 **canine HSAs**

413 In canine HSAs, *TP53* (n = 24/74; 32.4%), *PIK3CA* (n = 16/74; 21.6%), *PIK3R1* (n = 5/74;
414 6.8%), and *NRAS* (n = 4/74; 5.4%) transcripts showed recurrent mutations that were consistent

415 with those identified using tumor:normal Exome-sequencing (17). We found associations
416 between mutations of *TP53* (*TP53*^{mt}) and *PIK3CA* (*PIK3CA*^{mt}) and fusion genes (Fusion^{+})
417 (**Supplementary Table S8**). Specifically, *TP53*^{mt} commonly co-occurred with *PIK3CA*^{mt} (P =
418 0.004) and with fusion genes (P = 0.004); and Fusion^{+} tumors were seen in the tumors with
419 *TP53*^{mt} or *PIK3CA*^{mt} (P = 0.005) more frequently than would be expected by random chance.
420 When fusion genes co-occurred with *PIK3CA*^{mt}, they invariably co-occurred with mutations of
421 *TP53* (P = 0.037), and they were not associated with *PIK3CA*^{mt} alone (P = 0.324).
422 Next, we sought to determine if fusion genes were preferentially associated with specific
423 molecular subtypes of canine HSA. We previously defined distinct angiogenic, inflammatory,
424 and adipogenic molecular subtypes of canine HSA (21). To further validate this classification,
425 we applied unsupervised principal component analysis (PCA) and hierarchical clustering to
426 identify distinct groups in the sample cohort from this study (**Supplementary Fig. S6**). Our
427 results show that the three molecular subtypes (58 angiogenic, 14 inflammatory, and 4
428 adipogenic) were reproducibly identified in the current dataset, as illustrated in the heatmap of
429 1,477 DEGs (FDR $P < 0.001$; fold change > |3|) shown in **Fig. 3D**. Interestingly, fusion genes
430 were present only in tumors of the angiogenic HSA subtype (P = 0.046). Likewise, *TP53*
431 mutations were identified in 23 of 56 (41.1%) angiogenic HSAs, and in one of 18 tumors from
432 the two other molecular subtypes (P = 0.008). The somatic variants of *TP53*, *PIK3CA*, *PIK3R1*,
433 and *NRAS* were found in 33 of 56 (58.9%) angiogenic HSAs, and in 3 of 18 (16.7%) tumors
434 from the two other subtypes (P = 0.002). The angiogenic subtype of HSA also showed
435 upregulation of *PECAM1* (*CD31*), *FLT1* (*VEGFR1*), *KDR* (*VEGFR2)*, and *FLT4* (*VEGFR3)*
436 compared to the other two HSA subtypes and to non-malignant hematomas (**Fig. 3E**). We found
437 that five of 32 dogs (16%) with angiogenic HSA lived longer than five months, while four of 10

438 dogs (40%) with inflammatory HSA survived longer than that (**Supplementary Fig. S7**).
439 Eighteen of 30 (60.0%) fusion partners, including protein kinase-encoding genes such as *FLT1*,
440 *PTK2*, and *AKT3,* showed higher levels of expression in HSAs compared to non-malignant
441 controls ($P < 0.05$; fold change in a range from 1.3 to 6.0) (**Fig. 3F**). Neither breed, sex, neuter
442 status, age, nor affected organs were associated with the presence of fusion genes
443 (**Supplementary Fig. S8**). There was also no association between the fusion events and
444 histological subtype or mitotic index (**Supplementary Table S9**).
445 Next, we analyzed DEGs (FDR $P < 0.05$; fold change > |2|) and gene pathways to
446 examine gene signatures enriched in HSAs that had both fusion genes and *TP53* mutations. We
447 classified tumors according to their mutations as summarized in **Supplementary Table S10**. Co-
448 occurrence of fusion genes with *TP53* mutations (i.e., $TP53^{mt}$/$Fusion^{+}$/$PIK3CA^{wt}$ or PF tumors)
449 was associated with angiogenic and vascular signaling with enrichment of genes in pathways
450 such as PI3K, VEGF, and PDGF (**Supplementary Table S11 - S13**). Thirteen genes that were
451 commonly enriched in PF tumors were associated with activation of WNT3A as an upstream
452 regulator (**Supplementary Fig. S9**). **Fig. 4** illustrates a model integrating the data from these
453 findings to highlight potential pathogenetic contributions of fusion genes and recurrent mutations
454 in canine HSA.
455

456 **Human ASs and canine HSAs establish molecular programs that activate convergent**
457 **signaling pathways**

458 To determine if the genetic and molecular features of human AS and canine HSAs contributed to
459 the activation of functional pathways, we performed IHC in eleven human AS tissues and in 44
460 canine HSAs (**Fig. 5**; **Supplementary Tables S14** and **S15**). First, we evaluated the effects of

461 *TP53* mutation on the presence and location of p53, phospho-p53 (Ser15), and phospho-p53
462 (Ser20) (**Fig. 5A** and **B)**. In human ASs, nuclear expression of p53 was found in all of eleven
463 (100%) tumors, showing various levels of expression. Nuclear expression of phospho-p53
464 (Ser15) was seen in seven of eleven (63.6%) tumors, showing low expression in five of seven
465 (71%) tumors (IHC score ≤ 3). Nuclear and cytoplasmic expression of phospho-p53 (Ser20)
466 protein was detected in all eleven (100%) tumors, and seven of those showed high expression
467 (IHC score ≥ 7). In canine HSAs, p53 protein was localized to the nucleus in 34 of 44 (77%)
468 tumors with various levels of expression. Immunoreactivity of phospho-p53 (Ser15) was
469 observed in the nuclei of tumor cells in 38 of 40 (95%) cases, with 34 (90%) showing low or
470 medium expression (IHC score ≤ 6). Nuclear and cytoplasmic expression of phospho-p53
471 (Ser20) was seen in all of 40 HSAs (100%), with 32 tumors (80%) showing high levels of
472 expression. These data revealed that patterns of p53 and activated p53 were comparable in
473 human ASs and canine HSAs; especially, p53 was strongly phosphorylated at residue Ser20 in
474 tumors from both species. We found no association between phosphorylated p53 and *TP53*
475 mutations or fusion genes (**Supplementary Fig. S10**), suggesting that DNA damage and cellular
476 stress are widespread among these tumors, and they are likely to activate p53-mediated repair
477 mechanisms independent of these genetic alterations.
478 The PI3K/AKT/mTOR signaling pathway is important for regulation of angiogenic,
479 vascular, and energetic functions. To assess whether PI3K mutations resulted in higher levels of
480 downstream pathway activation, we evaluated expression of AKT and phospho-AKT proteins in
481 human ASs and canine HSAs (**Fig. 5C** and **D**). Expression of nuclear and cytoplasmic AKT
482 protein was observed in all eleven human ASs (100%) with eight of eleven (73%) tumors
483 showing medium or high expression. Expression of phospho-AKT (Thr308) was evaluated in

484 eight tumors; all of them (100%) showed weak or medium levels of expression. Similarly, AKT
485 protein was detectable in the nucleus and cytoplasm of all forty (100%) canine HSAs with 37
486 (93%) showing medium or high expression. Phospho-AKT (Thr308) was detected in the nuclei
487 and cytoplasm of all evaluable 39 (100%) canine HSAs, with 34 (87%) expressing medium or
488 high level of the protein. Strong AKT immunoreactivity was also seen in scattered stromal cells
489 in both human AS and canine HSA. Neither mutations of *TP53*, *PIK3CA*, *PIK3R1* nor the
490 presence of fusion genes were associated with expression of AKT and phospho-AKT in human
491 or canine tumors (**Supplementary Fig. S11**). Since *PIK3CA* and *PIK3R1* mutations were
492 undetectable in this set of eleven human ASs, we examined expression of mTOR and phospho-
493 mTOR (Ser2448) proteins as surrogates to confirm activation of their downstream pathways in
494 these tumors. mTOR protein was observed in the nuclei and cytoplasm of all eleven tumors (IHC
495 score ≥ 6), and it was not associated with the presence of *TP53* mutations or fusions
496 (**Supplementary Fig. S12A** and **B**). However, nuclear and cytoplasmic expression of phospho-
497 mTOR was higher in ASs that had *TP53* mutations or that had fusion genes than it was in tumors
498 without one of these genetic changes (**Supplementary Fig. S12C** and **D**). In summary, the
499 immunostaining data suggest that human AS and canine HSA have comparable activation of the
500 p53 and PI3K/AKT/mTOR pathways, and these events are largely independent of their
501 mutational states. Our results further suggest that these vasoformative tumors from both species
502 activate convergent signaling pathways that contribute to their final architecture and organization
503 with predictable enrichment of angiogenic gene signatures.
504

505 **Discussion**

506 For this study, our objective was to identify novel fusion genes in human ASs and spontaneous
507 canine HSAs. We showed that novel protein-coding fusion genes were identified in
508 approximately 50% of human ASs of which two had *TP53* mutations. In canine HSAs, protein-
509 coding fusion genes were detectable in ~15% of tumors, and those were associated with p53
510 deficiency and enrichment of angiogenic gene signatures. Our data suggest that convergent
511 molecular mechanisms associated with p53 inactivation and enhanced PI3K/AKT/mTOR
512 signaling pathways are operational in genomically complex human ASs and canine HSAs.
513
514 In the past decade, advances in next-generation sequencing and bioinformatics have
515 enabled genome-wide identification of unbiased cancer-associated fusion transcripts in a variety
516 of tumor types. Previous studies have reported 7,887 fusion transcripts identified across thirteen
517 tumor types in TCGA datasets and 9,928 fusion genes with a 3% recurrence rate in the Mitelman
518 Database of Chromosome Aberrations and Gene Fusions in Cancer (53-55). These findings
519 illustrate the complexity of the cancer-associated fusion gene landscape, showing a relatively
520 high rate of fusions with low recurrence, possibly arising from catastrophic chromosome
521 rearrangements by chromothripsis (56) and chromoplexy (57). Despite this relatively high
522 frequency of fusion genes, a solution to define their pathogenic significance remains elusive.
523 One key finding from this work was that protein-coding fusion genes co-occurred with mutations
524 of *TP53* in the angiogenic molecular subtype of canine HSA, suggesting that genomic instability
525 might create a predisposition for translocations and the resultant fusion genes and that, in turn,
526 these fusion genes create unique transcriptional programs that promote angiogenic phenotypes in
527 these p53-deficient backgrounds.
528

529 Specifically, kinase fusion genes involving *FLT1*, *PTK2*, and *AKT3* can activate key
530 convergent gene pathways associated with blood vessel formation and remodeling (58), and they
531 represent potential therapeutic targets for kinase inhibitors (35,59). When we consider that
532 sarcomas have the highest frequency of kinase fusions in TCGA datasets (35), but that they also
533 have extremely low recurrence, a more rational approach might be to develop agents that target
534 these convergent angiogenic pathways instead of the products from the individual fusion genes
535 themselves (60).
536
537 The two fusion genes that we confirmed by genomic structural evaluation in canine
538 HSAs were present in approximately 20 - 40% of cells in the tumor, both genes showing chaotic
539 amplification. Several explanations could account for these observations. One is that histology
540 and bioinformatics assays overestimated tumor content and tumor purity. Another is that fusions
541 are epiphenomena arising from chaotic genomes with no influence on selection. A third, which
542 we believe is most likely, is that translocation and the resulting fusion events occur stochastically
543 in genomically unstable cells late in the course of tumor evolution. However, the enrichment of
544 fusion genes and angiogenic transcriptional programs suggests that these traits endow tumor cells
545 with selective growth and/or survival advantages that contribute to tumor progression by
546 promoting proangiogenic environments. It is worth noting that the selective pressures in the AS
547 milieu favor not only fusion-positive clones, but also fusion-negative clones, as the establishment
548 of a proangiogenic environment could improve survival of all the subpopulations within the
549 tumor. Indeed, a similar mechanism might be operative in alveolar rhabdomyosarcomas, where
550 *PAX3-FOXO1A* fusions are necessary for tumor initiation but have no effect on tumor recurrence
551 (61,62). Further work will be necessary to distinguish which among these non-mutually

552 exclusive possibilities are operative, and to better understand the role of fusion genes in tumor
553 evolution of human AS and canine HSA and, potentially, in promoting clonal heterogeneity
554 through the creation of a permissive niche.
555
556 Fusion genes have been reported in human ASs (10,63-65). For instance, one study found
557 a *CIC-LEUTX* fusion in one of 120 (0.8%) FFPE ASs examined (10); another found a *CEP85L-*
558 *ROS1* fusion in one of 34 (3.0%) ASs examined (63); and a third found an *EWSR1-ATF1* fusion
559 in one case of AS (65). A *NUP160-SLC43A3* fusion has also been reported in the ISO-HAS AS
560 cell line (64). However, none of these fusion genes has been identified recurrently in subsequent
561 studies of AS samples. While these observations are consistent with our stochastic hypothesis,
562 we cannot completely exclude the possibility that fusion genes in human ASs, or for that matter
563 in canine HSAs, are non-pathogenic passenger aberrations.
564
565 A larger case series will be required to define the fusion gene landscape in human AS,
566 but canine HSA provides potential insights for what might be expected. Mutations of *TP53* are
567 largely mutually exclusive of mutations in *KDR*, *PIK3CA*, and *RAS* gene family in human AS,
568 and the mutational patterns seem to be associated with the location of the primary tumor
569 (10,12,17,66,67). We see a similar pattern emerge in a subset of canine HSA, and from our data
570 we propose a model that can be used as a foundation to test mechanistic links between the
571 mutational and transcriptional landscapes in malignant vascular tumors (**Fig. 4**) and determine
572 their roles in tumor progression. In this model, inflammatory HSAs harbor no mutations of
573 *PIK3CA*, and only rarely of *TP53*, maintaining sufficient genomic stability that disfavors
574 formation of fusion genes. Furthermore, the transcriptional programs in these inflammatory

575 HSAs are weakly angiogenic, and their permissive inflammatory environments restrain growth
576 and metastasis. Conversely, angiogenic HSAs harbor frequent mutations of *PIK3CA* and *TP53*,
577 and fusion events. Mutations of *PIK3CA* in p53-proficient backgrounds promote pro-angiogenic
578 environments, while in p53-deficient backgrounds, these mutations promote altered chromatin
579 regulation and immunomodulatory transcriptional programs. Finally, mutations of *TP53* enable
580 genomic instability with formation of fusion genes. These events are stochastic, but fusion genes
581 that promote pro-angiogenic transcriptional programs can enhance or even supplant the effects of
582 *PIK3CA* mutations and create environments that accelerate tumor growth and metastatic
583 propensity.

584 Molecular distinctions among human ASs could be driven by their clinical phenotype and
585 potential therapeutic responses (9,68,69). For instance, a subset of ASs harbor gene
586 amplifications of *MYC* and *FLT4* which frequently co-occur in tumors associated with ultraviolet
587 (UV) irradiation- or therapeutic radiation. Mutational signatures associated with UV exposure
588 and high mutational burden might predict more favorable immunotherapeutic responses in AS
589 patients, as they do in patients diagnosed with malignant melanoma; however, supportive clinical
590 trials to test this premise are limited, and the use of immune checkpoint inhibitors in human AS
591 patients thus far has yielded mixed results (70,71). The mutational signatures in canine HSA are
592 largely confined to the "aging" (cellular replication) signature (17), and total mutational burden
593 is relatively low (17,72), so this condition is unlikely to provide a model to address the utility of
594 immunotherapy in this context. However, canine HSA could provide a suitable model to address
595 other treatments, whether pharmacologic or immunologic, directed at the molecular programs
596 that drive progression and maintenance of the tumors in both species (33). Such validation

597 studies could alter the paradigms for diagnosis and treatment of human AS and canine HSA, as
598 well as of other aggressive, genomically complex sarcomas that affect humans and dogs alike.
599
600 **Data availability**
601 RNA-Seq gene expression data generated from human sarcomas are available from the TCGA
602 Research Network (https://www.cancer.gov/tcga). Exome sequencing data from human
603 angiosarcomas are available from The Angiosarcoma Project (https://ascproject.org), a project of
604 Count Me In (https://joincountmein.org/). RNA-Seq data from human AS tissues are available
605 through the Gene Expression Omnibus (GEO; http://www.ncbi.nlm. nih.gov/geo; accession
606 number GSE163359). RNA-Seq data from canine HSA tissues are published (17,21,32,33) and
607 available through the GEO (accession number GSE95183) and the NCBI Sequence Read
608 Archive (accession number PRJNA562916). All other data generated from this study are
609 available upon request to the corresponding author.
610
611 **Acknowledgements**
612 The authors would like to acknowledge Dr. Corrie Painter for reviewing the manuscript and
613 providing feedback. The authors acknowledge Mitzi Lewellen for assistance with inventory,
614 database management, and editorial assistance. The authors would also like to thank Lauren
615 Mills for processing of the next generation sequencing data and Dr. Douglas Yee, Director of
616 Masonic Cancer Center, for assisting with the collection of human tissues. Human biospecimens
617 were obtained from the UMN BioNet and from the CHTN. Tissue samples were provided by the
618 CHTN which is funded by the National Cancer Institute (NCI). Other investigators may have
619 received specimens form the same subjects. This work was partially supported by grants

620 1R03CA191713-01 (J.F. Modiano, A.L. Sarver, J.H. Kim) and R37CA218570 (E.K. Karlsson)
621 from the NCI of the National Institutes of Health (NIH), grants #422 (J.F. Modiano) and 1889-G
622 (J.F. Modiano, M. Breen, K. Lindblad-Toh) from the AKC Canine Health Foundation, grant
623 JHK15MN-004 (J.H. Kim) from the National Canine Cancer Foundation, grant D10-501 (J.F.
624 Modiano, M. Breen, K. Lindblad-Toh) from Morris Animal Foundation, and a grant from
625 Swedish Cancerfonden (K. Lindblad-Toh). This work was also supported by an NIH NCI R50
626 grant, CA211249 (A.L. Sarver). The NIH Comprehensive Cancer Center Support Grant to the
627 Masonic Cancer Center, University of Minnesota (P30 CA077598) provided support for the
628 cytogenetic analyses performed in the Cytogenomics Shared Resource. K. Megquier is supported
629 by the NCI of the NIH under Award Number F32CA247088. The content is solely the
630 responsibility of the authors and does not necessarily represent the official views of the NIH. M.
631 Breen is supported in part by the Oscar J. Fletcher Distinguished Professorship in Comparative
632 Oncology Genetics at North Carolina State University. K. Lindblad-Toh is supported by a
633 Distinguished Professor award from the Swedish Research Council. J.F. Modiano is supported
634 by the Alvin and June Perlman Chair in Animal Oncology. The UMGC
635 (http://genomics.umn.edu) supported for generation of genomic sequencing data libraries, and
636 the Minnesota Supercomputing Institute (MSI) at the University of Minnesota
637 (http://www.msi.umn.edu) provided computational resources that contributed to the results in
638 this study. The authors gratefully acknowledge donations to the Animal Cancer Care and
639 Research Program of the University of Minnesota that helped support this project.
640
641
642

643 **Disclosure of Potential Conflicts of Interest**

644 No potential conflicts of interest were disclosed.

645

646 **Authors' Contributions**

647 **Conception and design**: J.H. Kim, J.F. Modiano

648 **Development of methodology**: J.H. Kim, K. Megquier, A.L. Sarver, R. Thomas, J.F. Modiano

649 **Acquisition of data (provided animals, acquired and managed patients, provided facilities,**

650 **etc.)**: J.H. Kim, K. Megquier, R. Thomas, A.L. Sarver, N. Cheng, M.A. Linden, P. Murugan, L.

651 Oseth, C.L. Foster

652 **Analysis and interpretation of data (e.g., statistical analysis, biostatistics, computational**

653 **analysis)**: J.H. Kim, K. Megquier, R. Thomas, A.L. Sarver, J.M. Song, Y.T. Kim, N. Cheng,

654 M.A. Linden, P. Murugan, I. Elvers, R. Swofford, J. Turner-Maier, E.K. Karlsson, M. Breen, K.

655 Lindblad-Toh, J.F. Modiano

656 **Writing, review, and/or revision of the manuscript**: J.H. Kim, K. Megquier, R. Thomas, A.J.

657 Graef, K. Lindblad-Toh, J.F. Modiano with help from all authors

658 **Administrative, technical, or material support**: A.J. Graef

659 **Study supervision**: J.H. Kim, M. Breen, K. Lindblad-Toh, J.F. Modiano

660

661 **References**

662 1. Taylor BS, Barretina J, Maki RG, Antonescu CR, Singer S, Ladanyi M. Advances in

663 sarcoma genomics and new therapeutic targets. Nat Rev Cancer **2011**;11(8):541-57 doi

664 10.1038/nrc3087.

665 2. Neuville A, Ranchere-Vince D, Dei Tos AP, Montesco MC, Hostein I, Toffolatti L*, et al.*
666 Impact of molecular analysis on the final sarcoma diagnosis: a study on 763 cases
667 collected during a European epidemiological study. Am J Surg Pathol **2013**;37(8):1259-
668 68 doi 10.1097/PAS.0b013e31828f51b9.
669 3. Helman LJ, Meltzer P. Mechanisms of sarcoma development. Nat Rev Cancer
670 **2003**;3(9):685-94 doi 10.1038/nrc1168.
671 4. Italiano A, Chen CL, Thomas R, Breen M, Bonnet F, Sevenet N*, et al.* Alterations of the
672 p53 and PIK3CA/AKT/mTOR pathways in angiosarcomas: a pattern distinct from other
673 sarcomas with complex genomics. Cancer **2012**;118(23):5878-87 doi
674 10.1002/cncr.27614.
675 5. Buehler D, Rice SR, Moody JS, Rush P, Hafez GR, Attia S*, et al.* Angiosarcoma
676 outcomes and prognostic factors: a 25-year single institution experience. Am J Clin
677 Oncol **2014**;37(5):473-9 doi 10.1097/COC.0b013e31827e4e7b.
678 6. Lahat G, Dhuka AR, Hallevi H, Xiao L, Zou C, Smith KD*, et al.* Angiosarcoma: clinical
679 and molecular insights. Ann Surg **2010**;251(6):1098-106 doi
680 10.1097/SLA.0b013e3181dbb75a.
681 7. Fayette J, Martin E, Piperno-Neumann S, Le Cesne A, Robert C, Bonvalot S*, et al.*
682 Angiosarcomas, a heterogeneous group of sarcomas with specific behavior depending on
683 primary site: a retrospective study of 161 cases. Ann Oncol **2007**;18(12):2030-6 doi
684 10.1093/annonc/mdm381.
685 8. Smrke A, Hamm J, Karvat A, Simmons C, Srikanthan A. A retrospective review of 145
686 patients with angiosarcoma: Radiation therapy, extent of resection and chemotherapy are

687 important predictors of survival. Molecular and Clinical Oncology. Molecular and
688 Clinical Oncology **2020**;13:179-85 doi https://doi.org/10.3892/mco.2020.2055.
689 9. Behjati S, Tarpey PS, Sheldon H, Martincorena I, Van Loo P, Gundem G*, et al.*
690 Recurrent PTPRB and PLCG1 mutations in angiosarcoma. Nat Genet **2014**;46(4):376-9
691 doi 10.1038/ng.2921.
692 10. Huang SC, Zhang L, Sung YS, Chen CL, Kao YC, Agaram NP*, et al.* Recurrent CIC
693 Gene Abnormalities in Angiosarcomas: A Molecular Study of 120 Cases With
694 Concurrent Investigation of PLCG1, KDR, MYC, and FLT4 Gene Alterations. Am J
695 Surg Pathol **2016**;40(5):645-55 doi 10.1097/PAS.0000000000000582.
696 11. Antonescu CR, Yoshida A, Guo T, Chang NE, Zhang L, Agaram NP*, et al.* KDR
697 activating mutations in human angiosarcomas are sensitive to specific kinase inhibitors.
698 Cancer Res **2009**;69(18):7175-9 doi 10.1158/0008-5472.CAN-09-2068.
699 12. Painter CA, Jain E, Tomson BN, Dunphy M, Stoddard RE, Thomas BS*, et al.* The
700 Angiosarcoma Project: enabling genomic and clinical discoveries in a rare cancer through
701 patient-partnered research. Nat Med **2020**;26(2):181-7 doi 10.1038/s41591-019-0749-z.
702 13. Antonescu C. Malignant vascular tumors--an update. Mod Pathol **2014**;27 Suppl 1:S30-8
703 doi 10.1038/modpathol.2013.176.
704 14. Lamerato-Kozicki AR, Helm KM, Jubala CM, Cutter GR, Modiano JF. Canine
705 hemangiosarcoma originates from hematopoietic precursors with potential for endothelial
706 differentiation. Exp Hematol **2006**;34(7):870-8.
707 15. Cohen SM, Storer RD, Criswell KA, Doerrer NG, Dellarco VL, Pegg DG*, et al.*
708 Hemangiosarcoma in rodents: mode-of-action evaluation and human relevance. Toxicol
709 Sci **2009**;111(1):4-18 doi 10.1093/toxsci/kfp131.

710 16. Mullin C, Clifford CA. Histiocytic Sarcoma and Hemangiosarcoma Update. Vet Clin
711 North Am Small Anim Pract **2019**;49(5):855-79 doi 10.1016/j.cvsm.2019.04.009.
712 17. Megquier K, Turner-Maier J, Swofford R, Kim JH, Sarver AL, Wang C*, et al.*
713 Comparative Genomics Reveals Shared Mutational Landscape in Canine
714 Hemangiosarcoma and Human Angiosarcoma. Mol Cancer Res **2019**;17(12):2410-21 doi
715 10.1158/1541-7786.MCR-19-0221.
716 18. Wang G, Wu M, Durham AC, Radaelli E, Mason NJ, Xu X*, et al.* Molecular subtypes in
717 canine hemangiosarcoma reveal similarities with human angiosarcoma. PLoS One
718 **2020**;15(3):e0229728 doi 10.1371/journal.pone.0229728.
719 19. Thomas R, Borst L, Rotroff D, Motsinger-Reif A, Lindblad-Toh K, Modiano JF*, et al.*
720 Genomic profiling reveals extensive heterogeneity in somatic DNA copy number
721 aberrations of canine hemangiosarcoma. Chromosome Res **2014**;22(3):305-19 doi
722 10.1007/s10577-014-9406-z.
723 20. Andersen NJ, Nickoloff BJ, Dykema KJ, Boguslawski EA, Krivochenitser RI, Froman
724 RE*, et al.* Pharmacologic inhibition of MEK signaling prevents growth of canine
725 hemangiosarcoma. Mol Cancer Ther **2013**;12(9):1701-14 doi 10.1158/1535-7163.MCT-
726 12-0893.
727 21. Gorden BH, Kim JH, Sarver AL, Frantz AM, Breen M, Lindblad-Toh K*, et al.*
728 Identification of three molecular and functional subtypes in canine hemangiosarcoma
729 through gene expression profiling and progenitor cell characterization. Am J Pathol
730 **2014**;184(4):985-95 doi 10.1016/j.ajpath.2013.12.025.
731 22. Kim JH, Frantz AM, Sarver AL, Gorden Klukas BH, Lewellen M, O'Brien TD*, et al.*
732 Modulation of fatty acid metabolism and immune suppression are features of in vitro

733 tumour sphere formation in ontogenetically distinct dog cancers. Vet Comp Oncol
734 **2018**;16(1):E176-E84 doi 10.1111/vco.12368.
735 23. Hill R, Song Y, Cardiff RD, Van Dyke T. Selective evolution of stromal mesenchyme
736 with p53 loss in response to epithelial tumorigenesis. Cell **2005**;123(6):1001-11 doi
737 10.1016/j.cell.2005.09.030.
738 24. Goldstein I, Marcel V, Olivier M, Oren M, Rotter V, Hainaut P. Understanding wild-type
739 and mutant p53 activities in human cancer: new landmarks on the way to targeted
740 therapies. Cancer Gene Ther **2011**;18(1):2-11 doi 10.1038/cgt.2010.63.
741 25. Mitelman F, Johansson B, Mertens F. The impact of translocations and gene fusions on
742 cancer causation. Nat Rev Cancer **2007**;7(4):233-45 doi 10.1038/nrc2091.
743 26. Fosmire SP, Dickerson EB, Scott AM, Bianco SR, Pettengill MJ, Meylemans H*, et al.*
744 Canine malignant hemangiosarcoma as a model of primitive angiogenic endothelium.
745 Lab Invest **2004**;84(5):562-72.
746 27. Dickerson EB, Thomas R, Fosmire SP, Lamerato-Kozicki AR, Bianco SR, Wojcieszyn
747 JW*, et al.* Mutations of phosphatase and tensin homolog deleted from chromosome 10 in
748 canine hemangiosarcoma. Vet Pathol **2005**;42(5):618-32 doi 10.1354/vp.42-5-618.
749 28. Tamburini BA, Trapp S, Phang TL, Schappa JT, Hunter LE, Modiano JF. Gene
750 expression profiles of sporadic canine hemangiosarcoma are uniquely associated with
751 breed. PLoS One **2009**;4(5):e5549 doi 10.1371/journal.pone.0005549.
752 29. Kim J-H, Graef A, Dickerson E, Modiano J. Pathobiology of Hemangiosarcoma in Dogs:
753 Research Advances and Future Perspectives. Veterinary Sciences **2015**;2(4):388.

754 30. Rudolph P, Peters J, Lorenz D, Schmidt D, Parwaresch R. Correlation between mitotic
755 and Ki-67 labeling indices in paraffin-embedded carcinoma specimens. Hum Pathol
756 **1998**;29(11):1216-22.
757 31. Tschida BR, Temiz NA, Kuka TP, Lee LA, Riordan JD, Tierrablanca CA*, et al.* Sleeping
758 Beauty Insertional Mutagenesis in Mice Identifies Drivers of Steatosis-Associated
759 Hepatic Tumors. Cancer Res **2017**;77(23):6576-88 doi 10.1158/0008-5472.CAN-17-
760 2281.
761 32. Tonomura N, Elvers I, Thomas R, Megquier K, Turner-Maier J, Howald C*, et al.*
762 Genome-wide association study identifies shared risk loci common to two malignancies
763 in golden retrievers. PLoS Genet **2015**;11(2):e1004922 doi
764 10.1371/journal.pgen.1004922.
765 33. Borgatti A, Koopmeiners JS, Sarver AL, Winter AL, Stuebner K, Todhunter D*, et al.*
766 Safe and Effective Sarcoma Therapy through Bispecific Targeting of EGFR and uPAR.
767 Mol Cancer Ther **2017**;16(5):956-65 doi 10.1158/1535-7163.MCT-16-0637.
768 34. McPherson A, Hormozdiari F, Zayed A, Giuliany R, Ha G, Sun MG*, et al.* deFuse: an
769 algorithm for gene fusion discovery in tumor RNA-Seq data. PLoS Comput Biol
770 **2011**;7(5):e1001138 doi 10.1371/journal.pcbi.1001138.
771 35. Stransky N, Cerami E, Schalm S, Kim JL, Lengauer C. The landscape of kinase fusions
772 in cancer. Nat Commun **2014**;5:4846 doi 10.1038/ncomms5846.
773 36. Haas BJ, Papanicolaou A, Yassour M, Grabherr M, Blood PD, Bowden J*, et al.* De novo
774 transcript sequence reconstruction from RNA-seq using the Trinity platform for reference
775 generation and analysis. Nat Protoc **2013**;8(8):1494-512 doi 10.1038/nprot.2013.084.

776 37. Yoshihara K, Shahmoradgoli M, Martinez E, Vegesna R, Kim H, Torres-Garcia W*, et al.*
777 Inferring tumour purity and stromal and immune cell admixture from expression data.
778 Nat Commun **2013**;4:2612 doi 10.1038/ncomms3612.
779 38. Aran D, Hu Z, Butte AJ. xCell: digitally portraying the tissue cellular heterogeneity
780 landscape. Genome Biol **2017**;18(1):220 doi 10.1186/s13059-017-1349-1.
781 39. Kim JH, Frantz AM, Anderson KL, Graef AJ, Scott MC, Robinson S*, et al.* Interleukin-8
782 promotes canine hemangiosarcoma growth by regulating the tumor microenvironment.
783 Experimental cell research **2014**;323(1):155-64 doi 10.1016/j.yexcr.2014.02.020.
784 40. Anderson KL, Snyder KM, Ito D, Lins DC, Mills LJ, Weiskopf K*, et al.* Evolutionarily
785 conserved resistance to phagocytosis observed in melanoma cells is insensitive to
786 upregulation of pro-phagocytic signals and to CD47 blockade. Melanoma Res
787 **2020**;30(2):147-58 doi 10.1097/CMR.0000000000000629.
788 41. Thomas R, Duke SE, Karlsson EK, Evans A, Ellis P, Lindblad-Toh K*, et al.* A genome
789 assembly-integrated dog 1 Mb BAC microarray: a cytogenetic resource for canine cancer
790 studies and comparative genomic analysis. Cytogenet Genome Res **2008**;122(2):110-21
791 doi 10.1159/000163088.
792 42. Dobin A, Davis CA, Schlesinger F, Drenkow J, Zaleski C, Jha S*, et al.* STAR: ultrafast
793 universal RNA-seq aligner. Bioinformatics **2013**;29(1):15-21 doi
794 10.1093/bioinformatics/bts635.
795 43. Haas B, Dobin A, Stransky N, Li B, Yang X, Tickle T*, et al.* 2017 STAR-Fusion: Fast
796 and Accurate Fusion Transcript Detection from RNA-Seq. bioRxiv
797 <https://www.biorxiv.org/content/early/2017/03/24/120295>.

798 44. Li H, Handsaker B, Wysoker A, Fennell T, Ruan J, Homer N*, et al.* The Sequence
799 Alignment/Map format and SAMtools. Bioinformatics **2009**;25(16):2078-9 doi
800 10.1093/bioinformatics/btp352.
801 45. Qian X, Khammanivong A, Song JM, Teferi F, Upadhyaya P, Dickerson E*, et al.* RNA-
802 sequencing studies identify genes differentially regulated during inflammation-driven
803 lung tumorigenesis and targeted by chemopreventive agents. Inflamm Res
804 **2015**;64(5):343-61 doi 10.1007/s00011-015-0815-z.
805 46. Ashburner M, Ball CA, Blake JA, Botstein D, Butler H, Cherry JM*, et al.* Gene ontology:
806 tool for the unification of biology. The Gene Ontology Consortium. Nat Genet
807 **2000**;25(1):25-9 doi 10.1038/75556.
808 47. The Gene Ontology C. The Gene Ontology Resource: 20 years and still GOing strong.
809 Nucleic Acids Res **2019**;47(D1):D330-D8 doi 10.1093/nar/gky1055.
810 48. Mi H, Muruganujan A, Ebert D, Huang X, Thomas PD. PANTHER version 14: more
811 genomes, a new PANTHER GO-slim and improvements in enrichment analysis tools.
812 Nucleic Acids Res **2019**;47(D1):D419-D26 doi 10.1093/nar/gky1038.
813 49. Rodriguez AM, Graef AJ, LeVine DN, Cohen IR, Modiano JF, Kim JH. Association of
814 Sphingosine-1-phosphate (S1P)/S1P Receptor-1 Pathway with Cell Proliferation and
815 Survival in Canine Hemangiosarcoma. J Vet Intern Med **2015**;29(4):1088-97 doi
816 10.1111/jvim.13570.
817 50. Ronald L. Wasserstein, Lazar NA. The ASA's Statement on p-Values: Context, Process,
818 and Purpose. The American Statistician **2016**;70(2):129-33 doi
819 10.1080/00031305.2016.1154108.

820 51. Breen M, Modiano JF. Evolutionarily conserved cytogenetic changes in hematological
821 malignancies of dogs and humans--man and his best friend share more than
822 companionship. Chromosome Res **2008**;16(1):145-54 doi 10.1007/s10577-007-1212-4.
823 52. Marley K, Maier CS, Helfand SC. Phosphotyrosine enrichment identifies focal adhesion
824 kinase and other tyrosine kinases for targeting in canine hemangiosarcoma. Vet Comp
825 Oncol **2012**;10(3):214-22 doi 10.1111/j.1476-5829.2012.00325.x.
826 53. Mertens F, Johansson B, Fioretos T, Mitelman F. The emerging complexity of gene
827 fusions in cancer. Nat Rev Cancer **2015**;15(6):371-81 doi 10.1038/nrc3947.
828 54. Yoshihara K, Wang Q, Torres-Garcia W, Zheng S, Vegesna R, Kim H*, et al.* The
829 landscape and therapeutic relevance of cancer-associated transcript fusions. Oncogene
830 **2015**;34(37):4845-54 doi 10.1038/onc.2014.406.
831 55. Mitelman F, Johansson B, Mertens F. 2020 Mitelman Database Chromosome Aberrations
832 and Gene Fusions in Cancer. <https://mitelmandatabase.isb-cgc.org/>.
833 56. Stephens PJ, Greenman CD, Fu B, Yang F, Bignell GR, Mudie LJ*, et al.* Massive
834 genomic rearrangement acquired in a single catastrophic event during cancer
835 development. Cell **2011**;144(1):27-40 doi 10.1016/j.cell.2010.11.055.
836 57. Anderson ND, de Borja R, Young MD, Fuligni F, Rosic A, Roberts ND*, et al.*
837 Rearrangement bursts generate canonical gene fusions in bone and soft tissue tumors.
838 Science **2018**;361(6405) doi 10.1126/science.aam8419.
839 58. Lee HK, Chauhan SK, Kay E, Dana R. Flt-1 regulates vascular endothelial cell migration
840 via a protein tyrosine kinase-7-dependent pathway. Blood **2011**;117(21):5762-71 doi
841 10.1182/blood-2010-09-306928.

842 59. Kim P, Jia P, Zhao Z. Kinase impact assessment in the landscape of fusion genes that
843 retain kinase domains: a pan-cancer study. Brief Bioinform **2018**;19(3):450-60 doi
844 10.1093/bib/bbw127.
845 60. Medves S, Demoulin JB. Tyrosine kinase gene fusions in cancer: translating mechanisms
846 into targeted therapies. J Cell Mol Med **2012**;16(2):237-48 doi 10.1111/j.1582-
847 4934.2011.01415.x.
848 61. Pandey PR, Chatterjee B, Olanich ME, Khan J, Miettinen MM, Hewitt SM*, et al.* PAX3-
849 FOXO1 is essential for tumour initiation and maintenance but not recurrence in a human
850 myoblast model of rhabdomyosarcoma. J Pathol **2017**;241(5):626-37 doi
851 10.1002/path.4867.
852 62. Selfe JL, Shipley J. Fusion gene addiction: can tumours be forced to give up the habit? J
853 Pathol **2017**;242(3):263-6 doi 10.1002/path.4902.
854 63. Giacomini CP, Sun S, Varma S, Shain AH, Giacomini MM, Balagtas J*, et al.* Breakpoint
855 analysis of transcriptional and genomic profiles uncovers novel gene fusions spanning
856 multiple human cancer types. PLoS Genet **2013**;9(4):e1003464 doi
857 10.1371/journal.pgen.1003464.
858 64. Shimozono N, Jinnin M, Masuzawa M, Masuzawa M, Wang Z, Hirano A*, et al.*
859 NUP160-SLC43A3 is a novel recurrent fusion oncogene in angiosarcoma. Cancer Res
860 **2015**;75(21):4458-65 doi 10.1158/0008-5472.CAN-15-0418.
861 65. Gru AA, Becker N, Pfeifer JD. Angiosarcoma of the parotid gland with a t(12;22)
862 translocation creating a EWSR1-ATF1 fusion: a diagnostic dilemma. J Clin Pathol
863 **2013**;66(5):452-4 doi 10.1136/jclinpath-2012-201433.

864 66. Guo T, Zhang L, Chang NE, Singer S, Maki RG, Antonescu CR. Consistent MYC and
865 FLT4 gene amplification in radiation-induced angiosarcoma but not in other radiation-
866 associated atypical vascular lesions. Genes Chromosomes Cancer **2011**;50(1):25-33 doi
867 10.1002/gcc.20827.
868 67. Cornejo KM, Deng A, Wu H, Cosar EF, Khan A, St Cyr M*, et al.* The utility of MYC and
869 FLT4 in the diagnosis and treatment of postradiation atypical vascular lesion and
870 angiosarcoma of the breast. Hum Pathol **2015**;46(6):868-75 doi
871 10.1016/j.humpath.2015.02.014.
872 68. Beca F, Krings G, Chen YY, Hosfield EM, Vohra P, Sibley RK*, et al.* Primary mammary
873 angiosarcomas harbor frequent mutations in KDR and PIK3CA and show evidence of
874 distinct pathogenesis. Mod Pathol **2020**;33(8):1518-26 doi 10.1038/s41379-020-0511-6.
875 69. Chan JY, Lim JQ, Yeong J, Ravi V, Guan P, Boot A*, et al.* Multiomic analysis and
876 immunoprofiling reveal distinct subtypes of human angiosarcoma. J Clin Invest
877 **2020**;130(11):5833-46 doi 10.1172/JCI139080.
878 70. Florou V, Rosenberg AE, Wieder E, Komanduri KV, Kolonias D, Uduman M*, et al.*
879 Angiosarcoma patients treated with immune checkpoint inhibitors: a case series of seven
880 patients from a single institution. J Immunother Cancer **2019**;7(1):213 doi
881 10.1186/s40425-019-0689-7.
882 71. Dancsok AR, Gao D, Lee AF, Steigen SE, Blay JY, Thomas DM*, et al.* Tumor-associated
883 macrophages and macrophage-related immune checkpoint expression in sarcomas.
884 Oncoimmunology **2020**;9(1):1747340 doi 10.1080/2162402X.2020.1747340.

885 72. Wang G, Wu M, Maloneyhuss MA, Wojcik J, Durham AC, Mason NJ*, et al.* Actionable
886 mutations in canine hemangiosarcoma. PLoS One **2017**;12(11):e0188667 doi
887 10.1371/journal.pone.0188667.
888

Table 1. Putative fusion genes identified in transcriptomic data of human ASs

Patient ID	Gene 1	Gene 2	Putative fusion gene	Gene 1 chromosome	Gene 2 chromosome	Gene 1 fusion location	Gene 2 fusion location	Fusion Type	Gene 1 Ensembl ID	Gene 2 Ensembl ID	Genomic break position in gene 1	Genomic break position in gene 2	Somatic variants
Patient 1	-	-	-	-	-	-	-	-	-	-	-	-	-
Patient 2	-	-	-	-	-	-	-	-	-	-	-	-	-
Patient 3	*VKORC1L1*	*STEAP1B*	*VKORC1L1-STEAP1B*	7	7	coding	coding	Intra-chromosomal	ENSG00000196715	ENSG00000105889	65873565	22419836	-
	PPP1R13B	*ATP5MPL*	*PPP1R13B-ATP5MPL*	14	14	coding	coding	Intra-chromosomal	ENSG00000088808	ENSG00000156411	103847299	103915189	
Patient 4	-	-	-	-	-	-	-	-	-	-	-	-	-
Patient 5	-	-	-	-	-	-	-	-	-	-	-	-	*HRAS*
Patient 6	-	-	-	-	-	-	-	-	-	-	-	-	-
Patient 7	*SMURF1*	*TMEM139*	*SMURF1-TMEM139*	*7*	*7*	coding	intron	Intra-chromosomal	ENSG00000198742	ENSG00000178826	99143726	143286424	*TP53*
	AGO2	*TRAPPC9*	*AGO2-TRAPPC9*	*8*	*8*	coding	coding	Intra-chromosomal	ENSG00000123908	ENSG00000167632	140635485	140451383	
Patient 8	-	-	-	-	-	-	-	-	-	-	-	-	*NRAS*
Patient 9	*PEMT*	*ANKRD6*	*PEMT-ANKRD6*	17	6	coding	utr5p	Inter-chromosomal	ENSG00000133027	ENSG00000135299	17577027	89433375	-
	CPD	*NSRP1*	*CPD-NSRP1*	17	17	coding	coding	Intra-chromosomal	ENSG00000108582	ENSG00000126653	30461311	30172542	
Patient 10	*SCLT1*	*NIPBL*	*SCLT1-NIPBL*	4	5	coding	coding	Inter-chromosomal	ENSG00000151466	ENSG00000164190	128888679	37057186	-
Patient 11	*TEX2*	*PECAM1*	*TEX2-PECAM1*	17	17	utr5p	utr5p	Intra-chromosomal	ENSG00000136478	ENSG00000261371	64263168	64390763	-
Patient 12	*ATP8A2*	*FLT1*	*ATP8A2-FLT1*	13	13	coding	coding	Intra-chromosomal	ENSG00000132932	ENSG00000102755	25968679	28357685	-
Patient 13	*IRF9*	*THTPA*	*IRF9-THTPA*	14	14	coding	coding	Intra-chromosomal	ENSG00000213928	ENSG00000259431	24164134	23558695	*TP53*

Table 2. Putative fusion genes identified in transcriptomic data of canine HSAs

Dog sample ID	Gene 1	Gene 2	Putative fusion gene	Gene 1 chromosome	Gene 2 chromosome	Gene 1 fusion location	Gene 2 fusion location	Fusion type	Gene 1 Ensembl ID	Gene 2 Ensembl ID	Genomic break position in gene 1	Genomic break position in gene 2	Somatic variants	
CHAD-B7	*PREX2*	*LPCAT1*	*PREX2-LPCAT1*	29	34	coding	coding	Inter-chromosomal	ENSCAFG00000007620	ENSCAFG00000010491	17653781	11166324	*TP53*	-
DHSA-1204	*AP4E1*	*BAIAP2*	*AP4E1-BAIAP2*	30	9	coding	coding	Inter-chromosomal	ENSCAFG00000015318	ENSCAFG00000005700	16748493	968509	*TP53*	-
	NOL10	*PTPRB*	*NOL10-PTPRB*	17	10	coding	coding	Inter-chromosomal	ENSCAFG00000003435	ENSCAFG00000000446	7515966	12372230		
DHSA-0906	*MYO16*	*PTK2*	*MYO16-PTK2*	22	13	coding	coding	Inter-chromosomal	ENSCAFG00000006050	ENSCAFG00000001217	57750807	35397284	*TP53*	-
	ATP9A	*SNX5*	*ATP9A-SNX5*	24	24	coding	coding	Intra-chromosomal	ENSCAFG00000011659	ENSCAFG00000005463	37856900	5096627		
DHSA1101	*GABRA3*	*FLT1*	*GABRA3-FLT1*	X	25	utr5p	coding	Inter-chromosomal	ENSCAFG00000019161	ENSCAFG00000006701	120379631	11232377	*TP53*	-
DHSA1407	*ANKH*	*ATG16L1*	*ANKH-ATG16L1*	4	25	coding	coding	Inter-chromosomal	ENSCAFG00000014290	ENSCAFG00000011752	88259666	44761299	-	-
DHSA1416	*LAMB1*	*CBLB*	*LAMB1-CBLB*	18	33	coding	coding	Inter-chromosomal	ENSCAFG00000025057	ENSCAFG00000009793	12675054	11259031	*TP53*	*PIK3CA*
DHSA1513	*PIK3AP1*	*REV3L*	*PIK3AP1-REV3L*	28	12	coding	coding	Inter-chromosomal	ENSCAFG00000008880	ENSCAFG00000003942	10085967	67953124	*TP53*	*PIK3CA*
	AKT3	*XPNPEP1*	*AKT3-XPNPEP1*	7	28	coding	coding	Inter-chromosomal	ENSCAFG00000015806	ENSCAFG00000010661	34778111	21321899		
DHSA-1015	*MRPS35*	*CACNA1C*	*MRPS35-CACNA1C*	27	27	coding	coding	Intra-chromosomal	ENSCAFG00000010963	ENSCAFG00000016051	20003244	44487698	-	*PIK3CA*
	CCDC172	*ABLIM1*	*CCDC172-ABLIM1*	28	28	coding	coding	Intra-chromosomal	ENSCAFG00000011803	ENSCAFG00000011513	26980198	25377079		
DHSA-0803	*COPS5*	*NCOA2*	*COPS5-NCOA2*	29	29	utr5p	utr5p	Intra-chromosomal	ENSCAFG00000007386	ENSCAFG00000007775	16578975	19448341	*TP53*	*PIK3CA*
DHSA-0805	*MSN*	*LUC7L2*	*MSN-LUC7L2*	X	16	coding	coding	Inter-chromosomal	ENSCAFG00000016607	ENSCAFG00000004069	50748329	9413652	*TP53*	*PIK3CA*
DHSA-1113	*RANBP3L*	*ARL15*	*RANBP3L-ARL15*	4	4	coding	coding	Intra-chromosomal	ENSCAFG00000018711	ENSCAFG00000018394	72325076	61484049	-	-

889 **Figures**

890 **Figure 1.** Identification of novel putative protein-coding fusion transcripts in human AS and
891 canine HSA. The *Circos* plots visualize fusion genes identified in human ASs (**A**, *n* = 13) and
892 canine HSA (**B**, *n* = 76). Bar graphs show DNA copy number alterations for each fusion partner
893 gene using publicly available Exome-sequencing data in an independent dataset of human AS
894 (**C**, *n* = 36; data retrieved from Ref (12)) and using oaCGH in a larger HSA dataset (**D**, *n* = 123;
895 data retrieved from Ref (19)).

896

897 **Figure 2.** Validation of fusion genes in canine HSA. **A,** *MYO16-PTK2* fusion gene track and
898 visualization of the breakpoint in UCSC Genome Browser (Canfam3.1). **B,** Sanger sequencing
899 result of the PCR product for *MYO16-PTK2* fusion gene. **C,** Schematic illustration of the
900 putative *MYO16-PTK2* fusion gene and designed FISH probes. **D,** Detection of the *MYO16-*
901 *PTK2* fusion gene on primary canine HSA tissue by FISH. In wild type cells an association
902 between BAC clones 183H20 (red) and 385H13 (green) can be appreciated, both showing
903 independent localization from 451H13 (aqua). A portion of tumor cells shows a breakage
904 within 451H13, with one half of that signal associating with 183H20, and independent of the
905 localization of 385H13 indicating the existence of the *MYO16-PTK2* fusion at the genomic level.
906 **E,** Arrows indicate the amplification of the *MYO16-PTK2* fusion gene. **F,** Detection of the
907 *GABRA3-FLT1* fusion gene by FISH. The *GABRA3-FLT1* fusion is identified by break-apart
908 FISH probes for proximal *FLT1* (clone 363B20; red) at CFA 25 and distal *FLT1* at CFA 25
909 (clone 235H9; green). Split *FLT1* genes indicate the fusion event identified by single color signal
910 (white arrows). Dual colors represent the intact *FLT1* gene (grey arrows). **G,** DNA amplification
911 of *FLT1* gene.

912

913 **Figure 3.** Fusion genes, mutations of somatic variants, and molecular subtypes of human AS (A-
914 C) and canine HSA (D-F). **A,** 1,237 differentially expressed genes were identified between
915 human ASs (n = 13) and non-malignant tissue samples (n = 6) (False Discovery Rate or FDR $P <$
916 0.05): 490 genes were upregulated and 747 genes were downregulated in ASs. Ten fusion genes
917 are marked as yellow bars in seven AS samples. Somatic variations in *TP53* (n = 2), *NRAS* (n =
918 1), and *HRAS* (n = 1) were found in four ASs. **B,** Box plots show gene expression of *PECAM1,*
919 *FLT1*, *KDR*, and *FLT4* representing vasculogenic and angiogenic functions in human ASs and
920 non-malignant tissues (two-tailed Mann-Whitney test). ***, $P < 0.001$. **C**, Bar graphs show the
921 relative expression of genes in human ASs normalized to the expression of non-malignant
922 tissues. Six of 20 genes where the P-value was less than 0.05 are displayed (two-tailed Welch's
923 T-test). **D,** Heatmap illustrates 1,477 significant differentially expressed genes among three
924 subtypes of canine HSA (n = 76) (FDR $P < 0.001$; Fold change > 3). Somatic variant analysis
925 identified mutations in *TP53* (n = 24), *PIK3CA* (n = 16), *PIK3R1* (n = 5), *NRAS* (n = 4), and
926 *ARPC1A* (n = 1). Grey bars indicate unavailable somatic variants data. Fifteen fusion genes are
927 marked as yellow bars in 11 HSA samples. **E,** Box plots display gene expression of *PECAM1,*
928 *FLT1*, *KDR*, and *FLT4* representing vasculogenic and angiogenic functions in subtypes of HSA
929 and non-malignant hematomas (two-tailed Mann-Whitney test). ****, $P < 0.0001$; ***, $P <$
930 0.001; **, $P < 0.01$; *, $P < 0.05$. **F**, Bar graphs show the relative expression of genes in canine
931 HSA normalized to the expression of hematomas. Eighteen of 30 genes where the P-value is less
932 than 0.05 are displayed (two-tailed Welch's T-test). Heatmaps (**A** and **D**) show unsupervised
933 hierarchical clustering (average linkage). Heatmap colors display mean-centered fold change

934 expression following log_2 transformation. Upregulated genes are presented in red and
935 downregulated genes are shown in green.
936
937 **Figure 4.** Hypothetical model for angiogenic pathogenesis of canine HSA.
938
939 **Figure 5.** Immunohistochemical expression of p53 and AKT proteins in human AS and canine
940 HSA. **A,** Bar graphs show the number of cases (y-axis) plotted as a function of IHC scores (x-
941 axis) for staining with anti-p53, anti-phosphorylated (p)-p53 (Ser15), and anti-p-p53 (Ser20)
942 antibodies in human ASs (Left panel) and canine HSAs (Right panel). **B,** Representative
943 photomicrographs show IHC staining of p53, p-p53 (Ser15), and p-p53 (Ser20) in human AS
944 (Left panel) and canine HSA tissues (Right panel). Bar graphs (**C**) for IHC scores of AKT and p-
945 AKT (Thr308) proteins and representative photomicrographs (**D**) are also displayed for human
946 ASs and canine HSAs. H&E = hematoxylin and eosin stain. IHC staining (Horseradish
947 peroxidase and hematoxylin counterstain). 200X magnification.

Figure 1

A Human Angiosarcoma

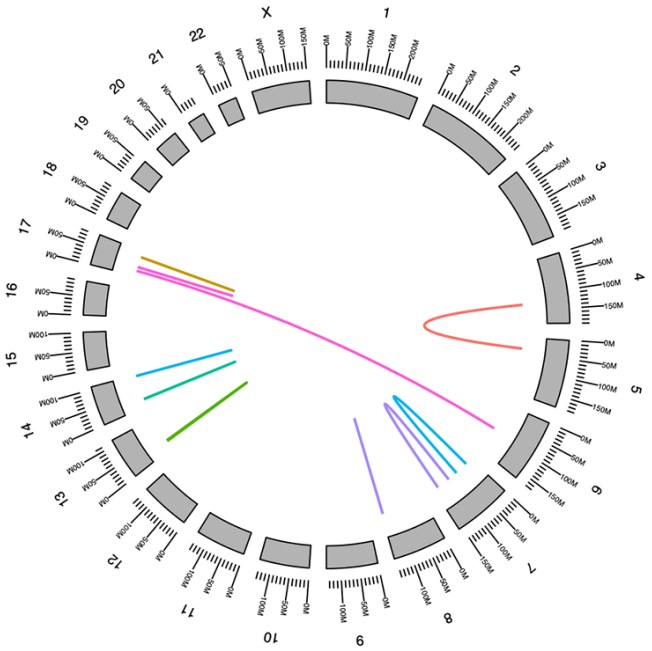

Sample ID	Fusion gene
Patient 3	*VKORC1L1-STEAP1B / PPP1R13B-ATP5MPL*
Patient 7	*SMURF1-TMEM139 / AGO2-TRAPPC9*
Patient 9	*PEMT-ANKRD6 / CPD-NSRP1*
Patient 10	*SCLT1-NIPBL*
Patient 11	*TEX2-PECAM1*
Patient 12	*ATP8A2-FLT1*
Patient 13	*IRF9-THTPA*

B Canine Hemangiosarcoma

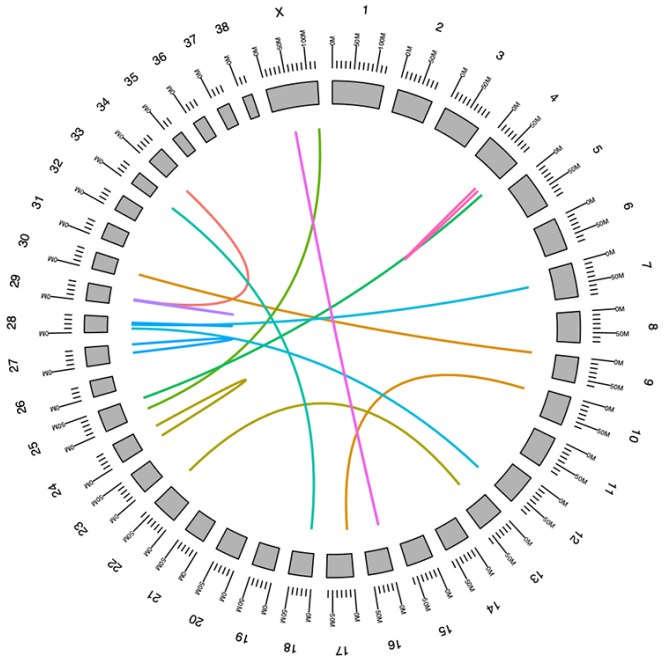

Sample ID	Fusion gene
CHAD-B7	*PREX2-LPCAT1*
DHSA-1204	*AP4E1-BAIAP2 / NOL10-PTPRB*
DHSA-0906	*MYO16-PTK2 / ATP9A-SNX5*
DHSA-1101	*GABRA3-FLT1*
DHSA-1407	*ANKH-ATG16L1*
DHSA-1416	*LAMB1-CBLB*
DHSA-1513	*PIK3AP1-REV3L / AKT3-XPNPEP1*
DHSA-1015	*MRPS35-CACNA1C / CCDC172-ABLIM1*
DHSA-0803	*COPS5-NCOA2*
DHSA-0805	*MSN-LUC7L2*
DHSA-1113	*RANBP3L-ARL15*

C

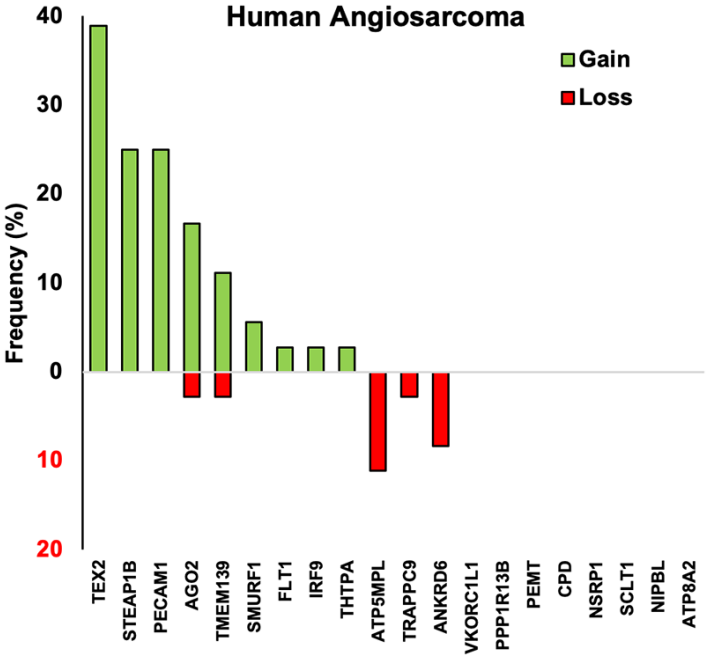

D

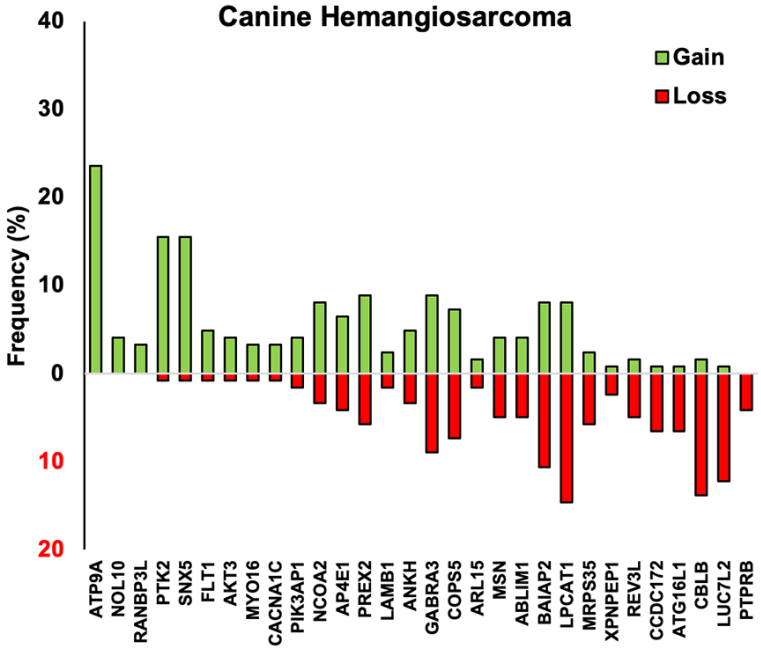

Figure 2

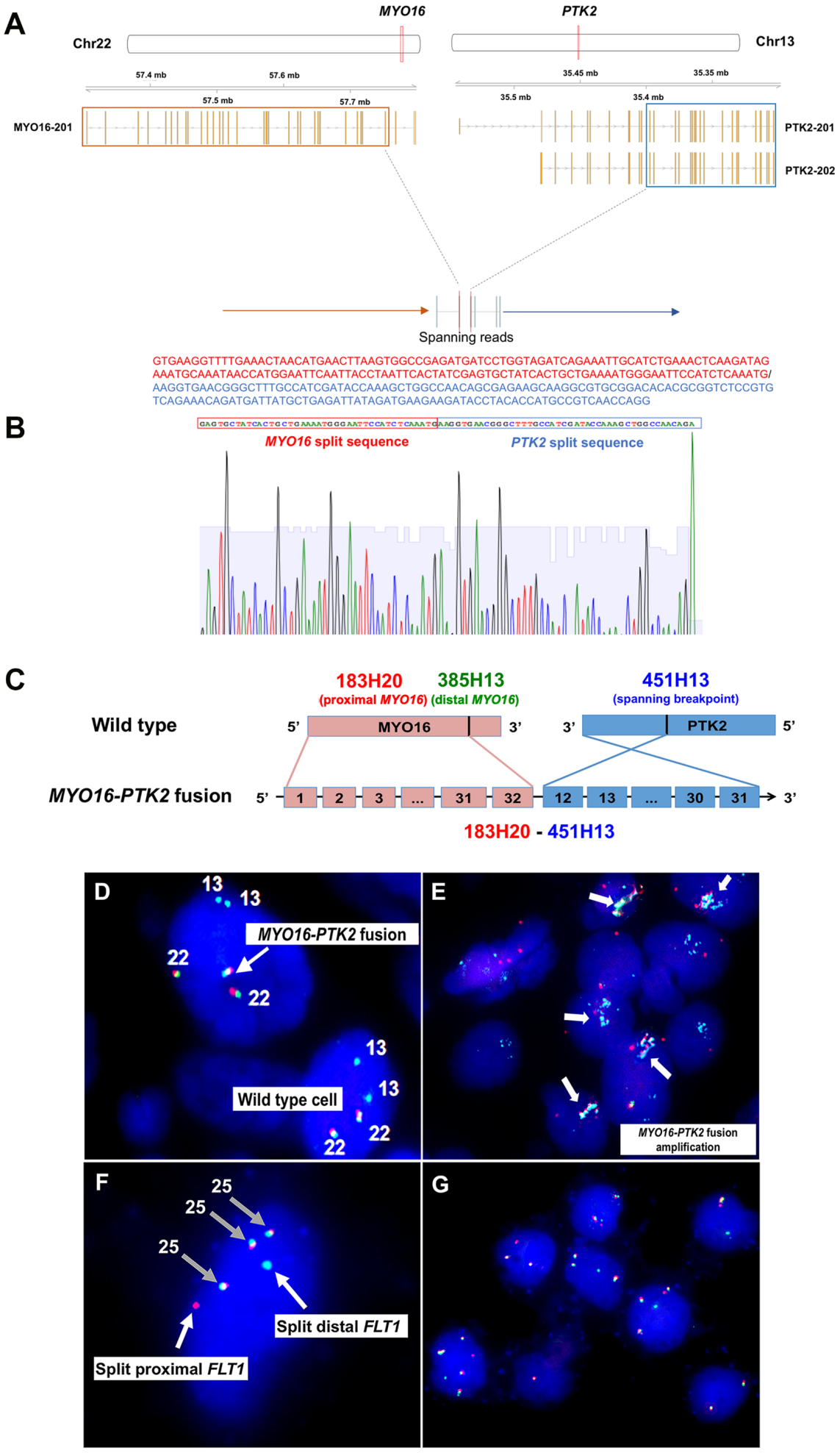
A
MYO16
PTK2
Chr22
Chr13
57.4 mb
57.6 mb
57.5 mb
57.7 mb
35.45 mb
35.35 mb
35.5 mb
35.4 mb
MYO16-201
PTK2-201
PTK2-202
Spanning reads
GTGAAGGTTTTGAAACTAACATGAACTTAAGTGGCCGAGATGATCCTGGTAGATCAGAAATTGCATCTGAAACTCAAGATAG
AAATGCAAATAACCATGGAATTCAATTACCTAATTCACTATCGAGTGCTATCACTGCTGAAAATGGGAATTCCATCTCAAATG/
AAGGTGAACGGGCTTTGCCATCGATACCAAAGCTGGCCAACAGCGAGAAGCAAGGCGTGCGGACACACGCGGTCTCCGTG
TCAGAAACAGATGATTATGCTGAGATTATAGATGAAGAAGATACCTACACCATGCCGTCAACCAGG
B
MYO16 split sequence
PTK2 split sequence
C
183H20
(proximal MYO16)
385H13
(distal MYO16)
451H13
(spanning breakpoint)
Wild type
5'
MYO16
3'
3'
PTK2
5'
MYO16-PTK2 fusion
5'
1
2
3
...
31
32
12
13
...
30
31
3'
183H20 - 451H13
D
13
13
MYO16-PTK2 fusion
22
22
13
13
Wild type cell
22
22
E
MYO16-PTK2 fusion amplification
F
25
25
25
Split distal FLT1
Split proximal FLT1
G

Figure 3

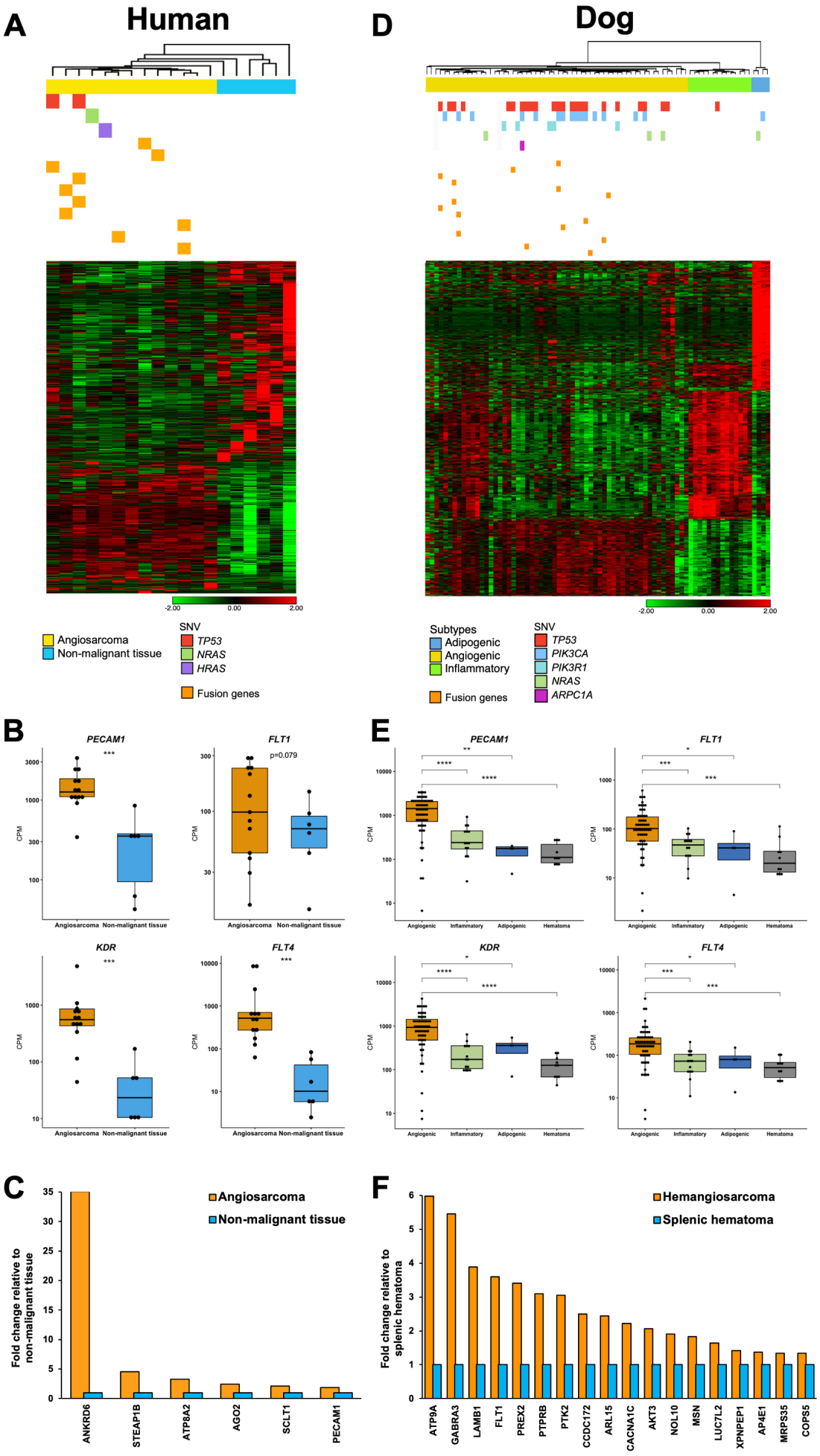
A
Human
Angiosarcoma
Non-malignant tissue
SNV
TP53
NRAS
HRAS
Fusion genes
D
Dog
Subtypes
Adipogenic
Angiogenic
Inflammatory
Fusion genes
SNV
TP53
PIK3CA
PIK3R1
NRAS
ARPC1A
B
PECAM1
FLT1
p=0.079
KDR
FLT4
CPM
Angiosarcoma
Non-malignant tissue
E
PECAM1
FLT1
KDR
FLT4
Angiogenic
Inflammatory
Adipogenic
Hematoma
C
Angiosarcoma
Non-malignant tissue
Fold change relative to non-malignant tissue
ANKRD6
STEAP1B
ATP8A2
AGO2
SCLT1
PECAM1
F
Hemangiosarcoma
Splenic hematoma
Fold change relative to splenic hematoma
ATP9A
GABRA3
LAMB1
FLT1
PREX2
PTPRB
PTK2
CCDC172
ARL15
CACNA1C
AKT3
NOL10
MSN
LUC7L2
XPNPEP1
AP4E1
MRPS35
COPS5

Figure 4

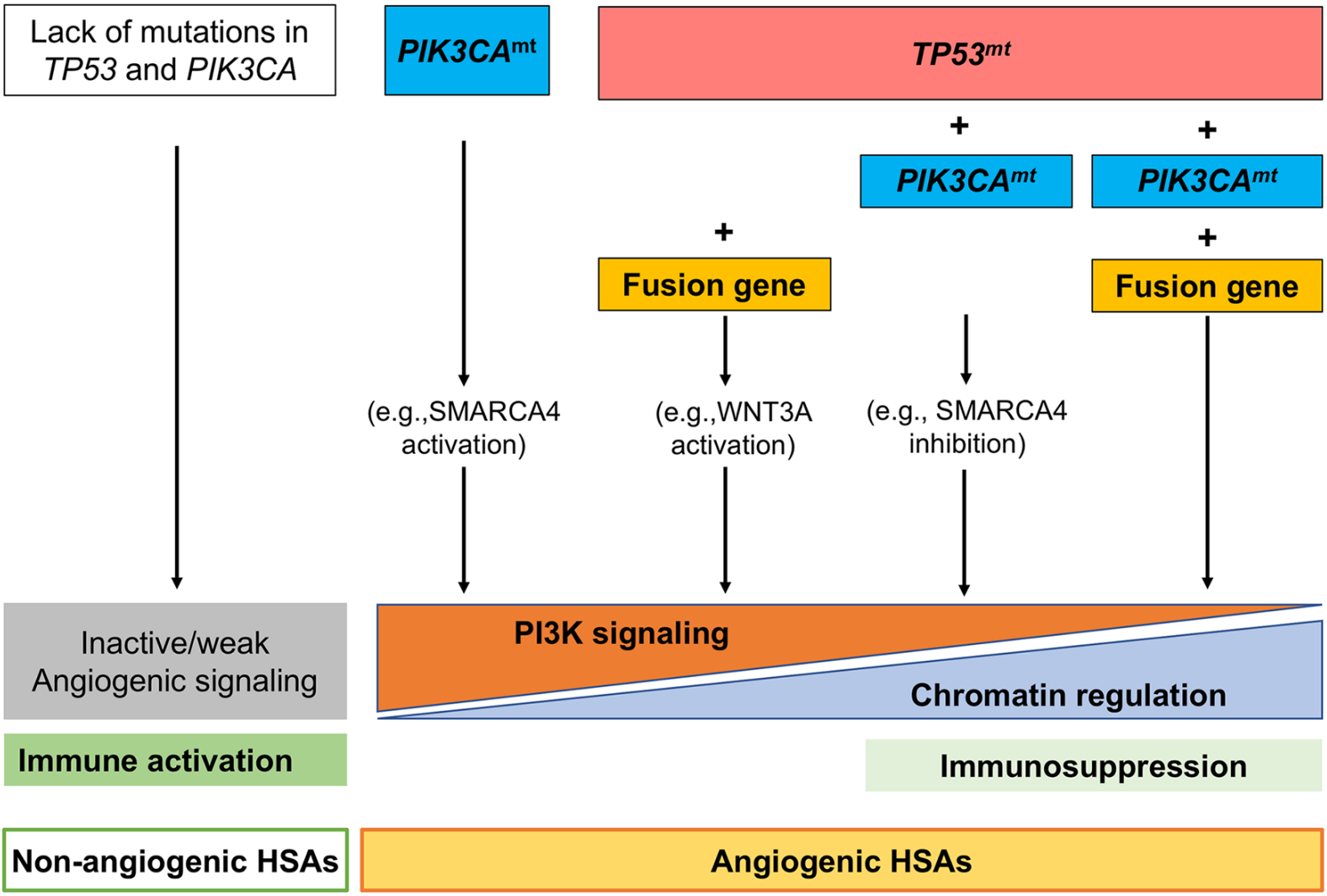
Lack of mutations in *TP53* and *PIK3CA*
*PIK3CA*mt
*TP53*mt
+
*PIK3CA*mt
+
*PIK3CA*mt
+
Fusion gene
+
Fusion gene
(e.g.,SMARCA4 activation)
(e.g.,WNT3A activation)
(e.g., SMARCA4 inhibition)
Inactive/weak Angiogenic signaling
PI3K signaling
Chromatin regulation
Immune activation
Immunosuppression
Non-angiogenic HSAs
Angiogenic HSAs

Figure 5

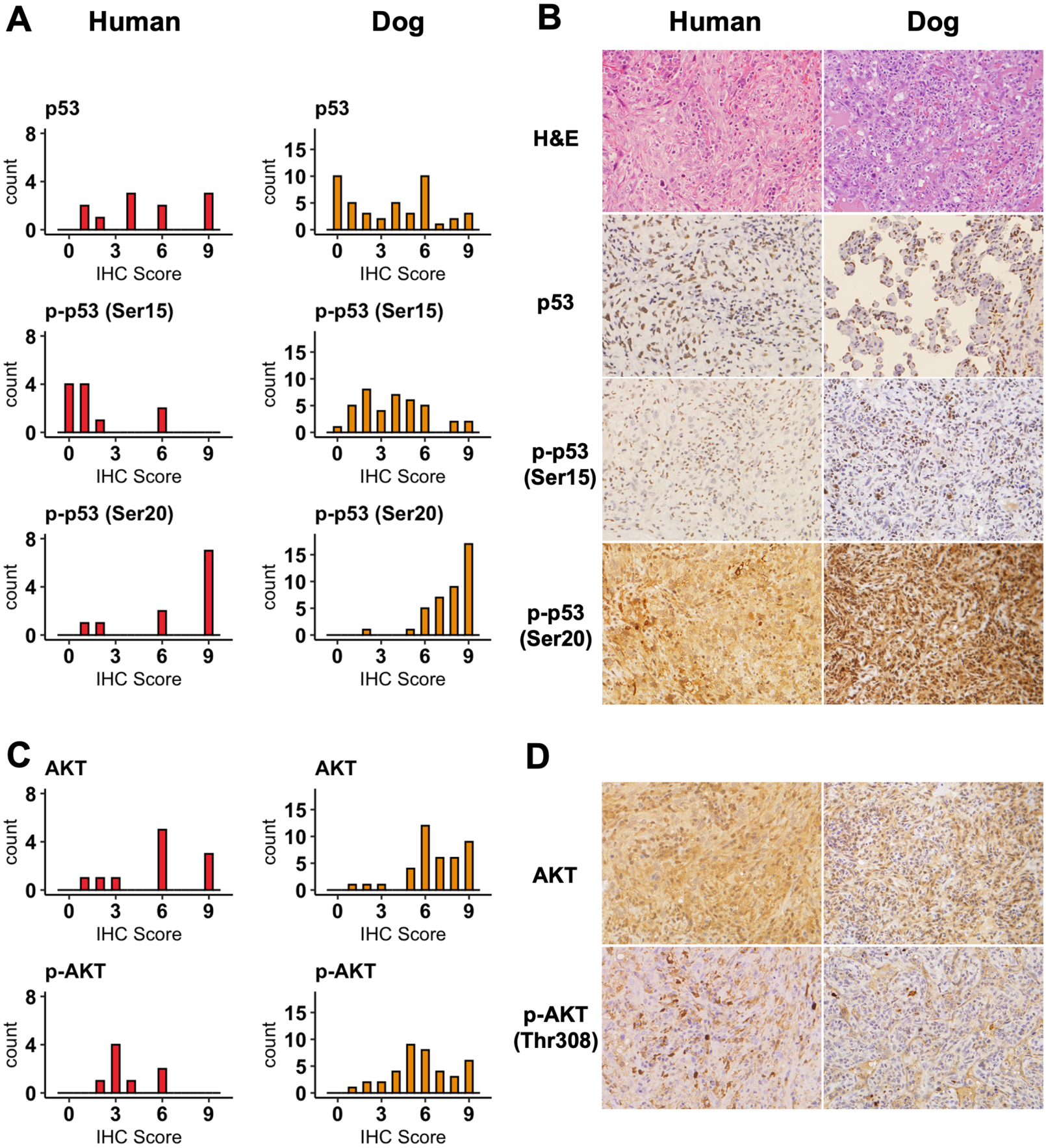
A
Human
Dog
p53
p-p53 (Ser15)
p-p53 (Ser20)
count
IHC Score
B
Human
Dog
H&E
p53
p-p53 (Ser15)
p-p53 (Ser20)
C
AKT
p-AKT
D
AKT
p-AKT (Thr308)